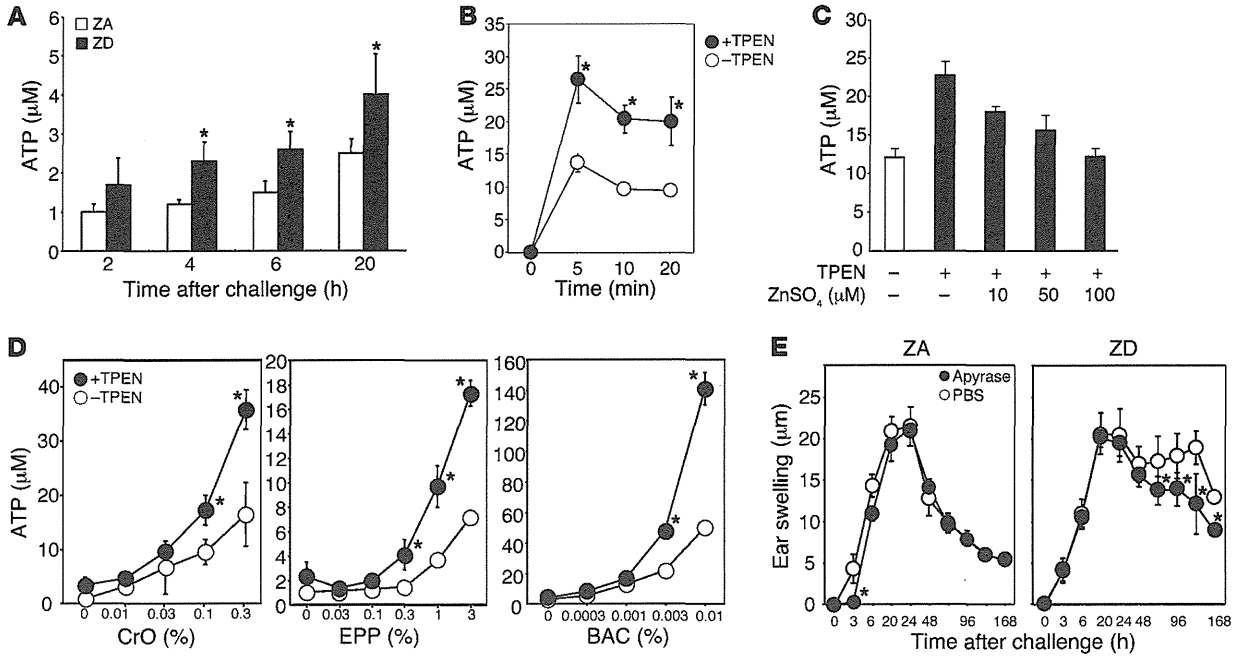

Figure 2

Zn deficiency increases ATP release by keratinocytes in response to irritant chemicals. (**A**) 1% CrO was painted on the ears of ZA (white bars) and ZD (black bars) mice ($n = 5$), and skin samples were taken at the indicated time points. ATP secretion from skin organ cultures was quantified. (**B–D**) Pam-212 keratinocytes were treated with (**B** and **C**) 0.3% CrO or (**D**) titrated concentrations of CrO, EPP, or BAC in the presence (black circles/bars) or absence (white circles/bars) of 2 μM TPEN. ATP in the culture supernatants was quantified at (**B**) the indicated time points or (**C** and **D**) 10 minutes after stimulation. (**C**) Cells were cultured with 10–100 μM $ZnSO_4$. *$P < 0.05$, compared with cells that were not treated with TPEN. (**E**) ICD responses to CrO were induced, as described in Figure 1. ZA and ZD mice ($n = 5$) received local injections of potato apyrase on the right ear (black circles) or PBS alone on the left ear (white circles) before and after CrO application to both ears. The data shown are the swelling responses (mean ± SD). *$P < 0.05$, between the apyrase and PBS treatments. Data are representative of 3 independent experiments.

irritant chemicals (herein, EPP and BAC) (Figure 2D). Together, these findings clearly indicate that Zn deficiency and irritant chemicals synergistically increase ATP release from keratinocytes.

Although various types of cells release ATP, the mechanism underlying the release of ATP is controversial (29). Several studies have shown that the release of ATP is reduced by carbenoxolone (CBX), suggesting the involvement of connexin or pannexin membrane channels in the release. In addition, inhibition of ATP release by vesicular ATPase inhibitors or intracellular Ca^{2+} deprivation was also reported, suggesting that the mechanisms of ATP release could include exocytosis. As shown in Supplemental Figure 3, CBX significantly decreased ATP release from CrO-treated keratinocytes, and, more importantly, it dramatically inhibited TPEN-mediated increase of ATP secretion. By contrast, BAPTA-AM, a membrane-permeable, strong Ca^{2+}-chelator, did not affect the CrO-evoked ATP release from keratinocytes. These results clearly indicate that membrane channel–mediated diffusible mechanisms, but not Ca^{2+}-dependent exocytosis, play a key role in the release of ATP from keratinocytes treated with CrO.

Previous studies have shown that hydrolysis of nucleotides by s.c. injections of soluble ecto-nucleoside triphosphate diphosphohydrolase (NTPDase; soluble potato apyrase) diminishes early inflammation in ICD (28). As shown in Figure 2E, we obtained similar results in ZA mice. In contrast, injections of apyrase before and after CrO application in ZD mice significantly decreased the late ICD response (Figure 2E). This suggests that aberrant ATP release from epidermal keratinocytes in response to irritant chemicals contributes, at least in part, to the prolonged ICD response in ZD mice.

Aberrant chemokine gene expression in ZD keratinocytes. In general, there are very few differences in the histological, immunohistochemical, and electron microscopy findings in ACD and ICD (30). However, ICD is thought to be mediated via T cell–independent innate immunity, because the ear swelling response to CrO is similar for both athymic and normal mice and neutrophils are the predominant cells in ICD (31). Recent work has shown that different patterns of inflammatory chemokines may distinguish between ACD and ICD (32). To explore such mechanisms for increased ICD in Zn deficiency, we first analyzed gene expression profiles for 44 chemokines in epidermal sheets obtained from ZA and ZD mice 24 hours after vehicle or CrO exposure. Profound differences in chemokine gene expression were observed (Supplemental Figure 4). However, *Cxcl1* was markedly induced by CrO in both ZA and ZD mice, suggesting a possible association between this chemokine and neutrophil recruitment. Because CXCL1 and CXCL2 are known to mediate neutrophil influx into tissues (33), we next quantified their mRNA expression in epidermal sheets obtained from ZA and ZD mice after vehicle or CrO application in vivo. Quantitative real-time PCR demonstrated that Zn deficiency resulted in a significant increase of *Cxcl1* mRNA 4 and 24 hours after CrO exposure and *Cxcl2* mRNA at 4 hours (Figure 3, A and B). The same enhancing effects of Zn deficiency for the chemokine mRNA expression were observed when mice were treated with BAC (Supplemental Figure 5A). In addition, in vitro exposure of Pam-

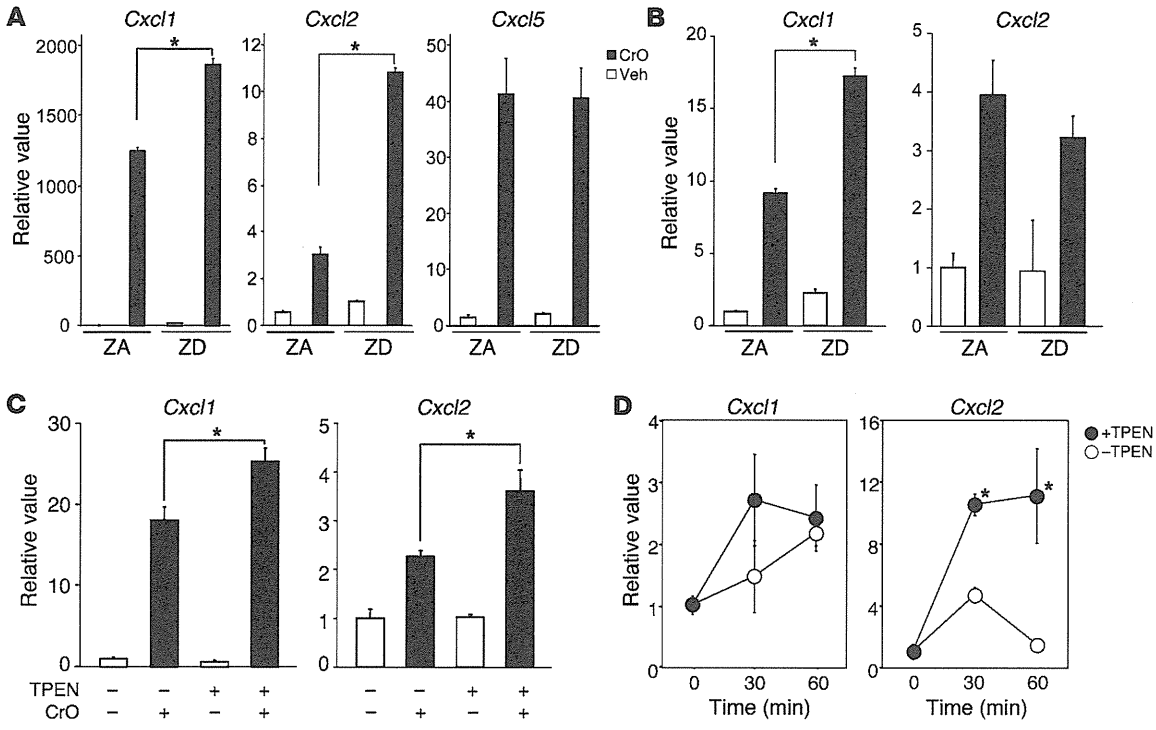

Figure 3

Zn deficiency increases *Cxcl1* and *Cxcl2* gene expression in keratinocytes after treatment with CrO. (**A** and **B**) 1% CrO (black bars) or vehicle alone (white bars) was painted on the ears of ZA and ZD mice ($n = 5$). Epithelial sheets were obtained from the ears at (**A**) 4 hours or (**B**) 24 hours, and total RNA was extracted. (**C**) Pam-212 keratinocytes were cultured in the presence or absence of 2 μM TPEN. Total RNA was extracted 4 hours after 0.3% CrO (black bars) or vehicle (white bars) exposure. (**D**) Pam-212 keratinocytes were treated with 100 μM ATPγS in the presence (black circles) or absence (white circles) of 2 μM TPEN. Total RNA was extracted 4 hours after ATPγS exposure. Quantitative real-time RT-PCR analysis of *Cxcl1* and *Cxcl2* was performed. *Cxcl5* was examined as control in **A**. mRNA expression was normalized to *Gapdh*. The fold induction (mean ± SD) was calculated from the normalized mRNA expression by CrO- or ATP-stimulated keratinocytes relative to nonstimulated ZA keratinocytes. *$P < 0.05$, compared with cells that were from ZA mice or not treated with TPEN. Data are representative of 3 independent experiments.

212 keratinocytes to CrO rapidly induced *Cxcl1* and *Cxcl2* mRNA (Figure 3C). When TPEN was added to the cultures, significant further augmentation of CrO-induced chemokine mRNA accumulation was observed, which was not seen with TPEN alone (Figure 3C). Similar results were obtained in BAC-treated keratinocytes (Supplemental Figure 5B). Furthermore, consistent with recent findings (34), exogenous ATPγS induced *Cxcl1* and *Cxcl2* mRNA expression by ZA Pam-212 keratinocytes (Figure 3D). Together, our results suggest that Zn deficiency indirectly augments *Cxcl1* and *Cxcl2* gene expression in CrO-stimulated keratinocytes via increased ATP release, as observed in Figure 2. Interestingly, Zn deficiency further augmented ATPγS-induced *Cxcl2*, but not *Cxcl1*, mRNA expression (Figure 3D).

Loss of epidermal Langerhans cells in Zn deficiency. Langerhans cells (LCs) are a long-lived subset of tissue DCs that reside in the epidermis. LCs acquire skin antigens and then migrate to skin-draining LNs in both inflammatory and steady-state conditions (35). Recently, it has been shown that CD39, which is expressed exclusively by LCs in the epidermal compartment, is responsible for ecto-NTPDase activity in LCs (28). Because the P2-receptor signaling pathway is negatively regulated by NTPDase-dependent hydrolysis of ATP, LC-associated CD39 plays a protective role against ATP-mediated inflammatory signals by hydrolyzing extracellular nucleotides released by keratinocytes in ICD responses (28). Therefore, we next examined the number, distribution, and morphology of epidermal LCs in Zn deficiency. Although epidermal cells prepared from the ear skin of ZA mice contained a normal contingent of LCs (I-A^{d+} $CD11c^+$ cells), in mice fed the ZD diet, the number of epidermal LCs decreased with time on the diet, and few LCs were observed after 6 weeks (Figure 4, A and B). Immunofluorescence microscopy confirmed the loss of LCs from epidermal sheets prepared from mice fed a ZD diet for 6 weeks (Figure 4C). In contrast, the frequency and morphology of dendritic epidermal T cells (DETCs; $Thy\text{-}1^+$ cells), which are skin-resident γδ T cells expressing a monoclonal T cell receptor containing Vγ3 and Vδ1 determinants, in ZD mice was normal even after 6 weeks (Figure 4, C and D). It is of note that the proportions of I-A^+ $CD11c^+$ cells in axillary and inguinal lymph nodes, including migratory DCs (e.g., LCs) and resident lymphoid DCs, from ZD mice were comparable in number to those of ZA mice (Figure 4A). The possibility that Zn deficiency downregulates the expression of cell surface markers on epidermal LCs was considered unlikely, because treatment of epidermal sheets with TPEN (2 μM) for 4 days failed to decrease surface expression of I-A^d and CD11c on murine epidermal LCs (data not shown).

Loss of epidermal LCs in patients with AE. We next examined the number, distribution, and morphology of epidermal LCs in human skin

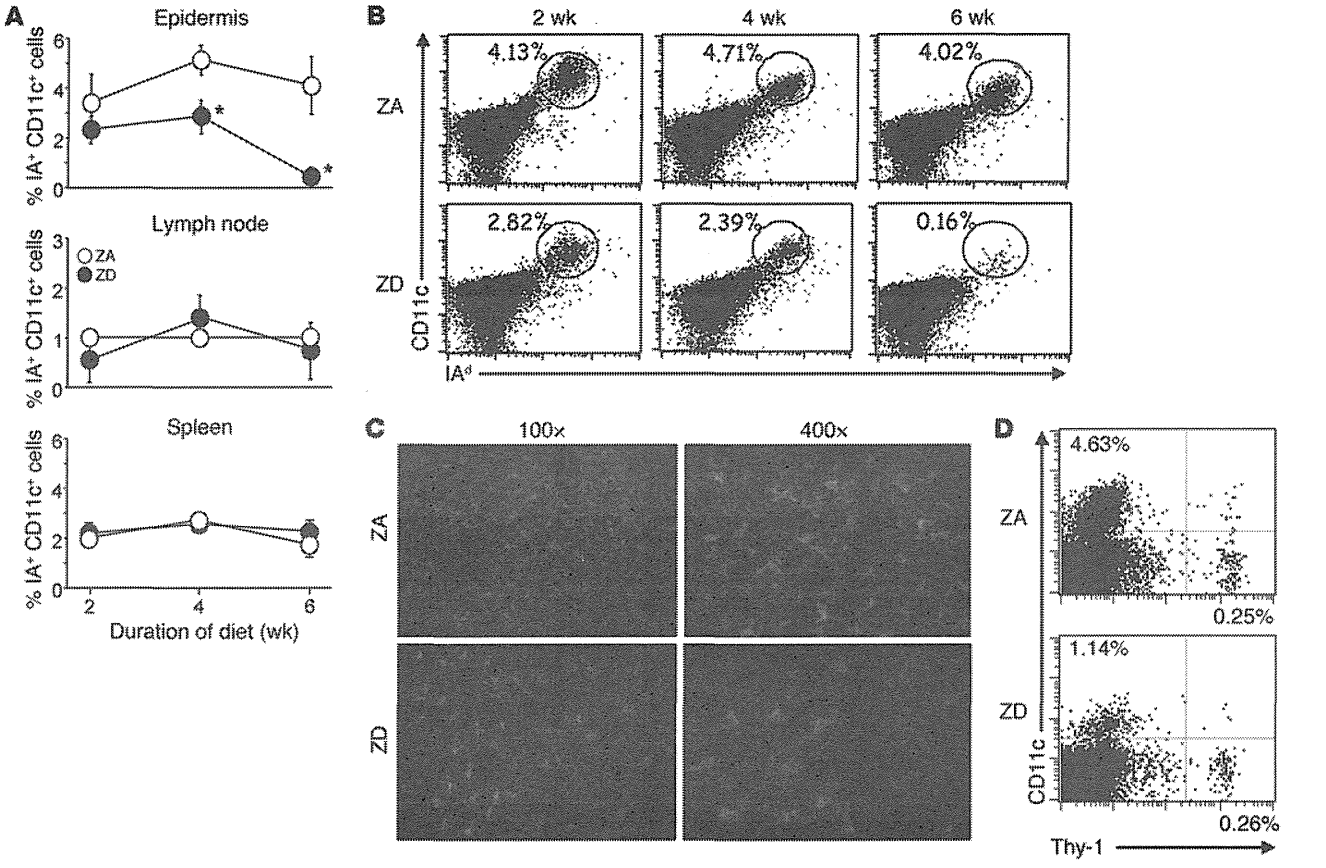

Figure 4

Loss of epidermal LCs in Zn deficiency. (**A**) Cell suspensions of epidermis, axillary, and inguinal lymph nodes and spleens were prepared from mice fed ZA (white circles) or ZD (black circles) diets for the indicated time and stained for I-A and CD11c antigens. The percentages of I-A and CD11c double-positive cells were assessed within each live-gated cell population. Results are the mean ± SD (n = 3). *P < 0.05, compared with mice fed the ZA diet. A representative FACS analysis of live-gated epidermal cell suspensions from mice fed ZA or ZD diets for 6 weeks and stained for (**B**) I-A and CD11c or (**D**) Thy-1 and CD11c antigens. Numbers indicate the percentages of cells in the (**B**) circles or (**D**) gate. (**C**) Immunofluorescence of epidermal whole mounts stained for I-A (red) and Thy-1 (green) from mice fed ZA or ZD diets for 6 weeks. Original magnification, ×100 (left panels); ×400 (right panels). Data are representative of 3 independent experiments.

samples obtained from inflammatory lesions of patients, including those with atopic dermatitis, psoriasis vulgaris, and hereditary and acquired AE, by immunofluorescence staining analyses. Langerin$^+$ LCs were found to be regularly scattered throughout the epidermis of control specimens but were absent from the epidermis of patients with AE (Figure 5A). HLA-DR antigens were also rarely expressed in the epidermis of AE specimens but were present on the surface of dermal mononuclear cells in the same specimens (Figure 5B). Interestingly, skin biopsy specimens obtained from the same lesions in a patient with hereditary AE after 6 months of oral Zn supplementation revealed recolonization of the epidermis with LCs, accompanied by marked clinical improvement (Figure 5C). We also examined immunohistochemical staining with formalin-fixed skin samples obtained from patients with AE. As shown in Supplemental Figure 6A, langerin$^+$ LCs were absent from the epidermis of the patients with AE. Quantitation of langerin$^+$ cells in the epidermis (n = 3) revealed that the number of LCs in the lesional epidermis of AE specimens was significantly decreased as compared with that in normal skin (the mean positive cell per field ± SD was 16.7 ± 2.8 in normal skin and 0.4 ± 0.3 in AE skin; P < 0.05). Similarly, the number of HLA-DR$^+$ cells in the lesional epidermis of AE specimens was also significantly decreased (the mean positive cell per field ± SD was 10.4 ± 0.6 in normal skin and 3.7 ± 2.7 in AE skin; P < 0.05). Taken together with the findings in ZD mice (Figure 4), these findings indicate that Zn deficiency results in depletion of epidermal LCs.

Decreased steady-state production of TGF-β1 in cutaneous, but not mucosal, epidermis in Zn deficiency. Although the mechanisms that regulate LC homeostasis in the steady state are yet to be fully elucidated, previous studies demonstrated that LC development requires TGF-β1 (35). Mice lacking TGF-β1 possess no LCs, owing to either a failure in LC differentiation, survival, or both (35, 36). Therefore, we next assessed the cutaneous expression of TGF-β1 in Zn deficiency. Mucosal TGF-β1 levels in the large and small intestine in ZD mice were comparable to those in ZA mice (Figure 6B), whereas the skin tissue obtained from ZD mice contained significantly lower amounts of TGF-β1 than that from ZA mice (Figure 6A). To detect the TGF-β activity in the skin samples, MFB-F11 reporter cells were used in a bioassay (Figure 6C and ref. 37). Secreted alkaline phosphatase (SEAP) activity was not detected without activation of the samples by HCl, suggesting that murine skin contains TGF-β protein in a latent form. However, after activation, skin samples

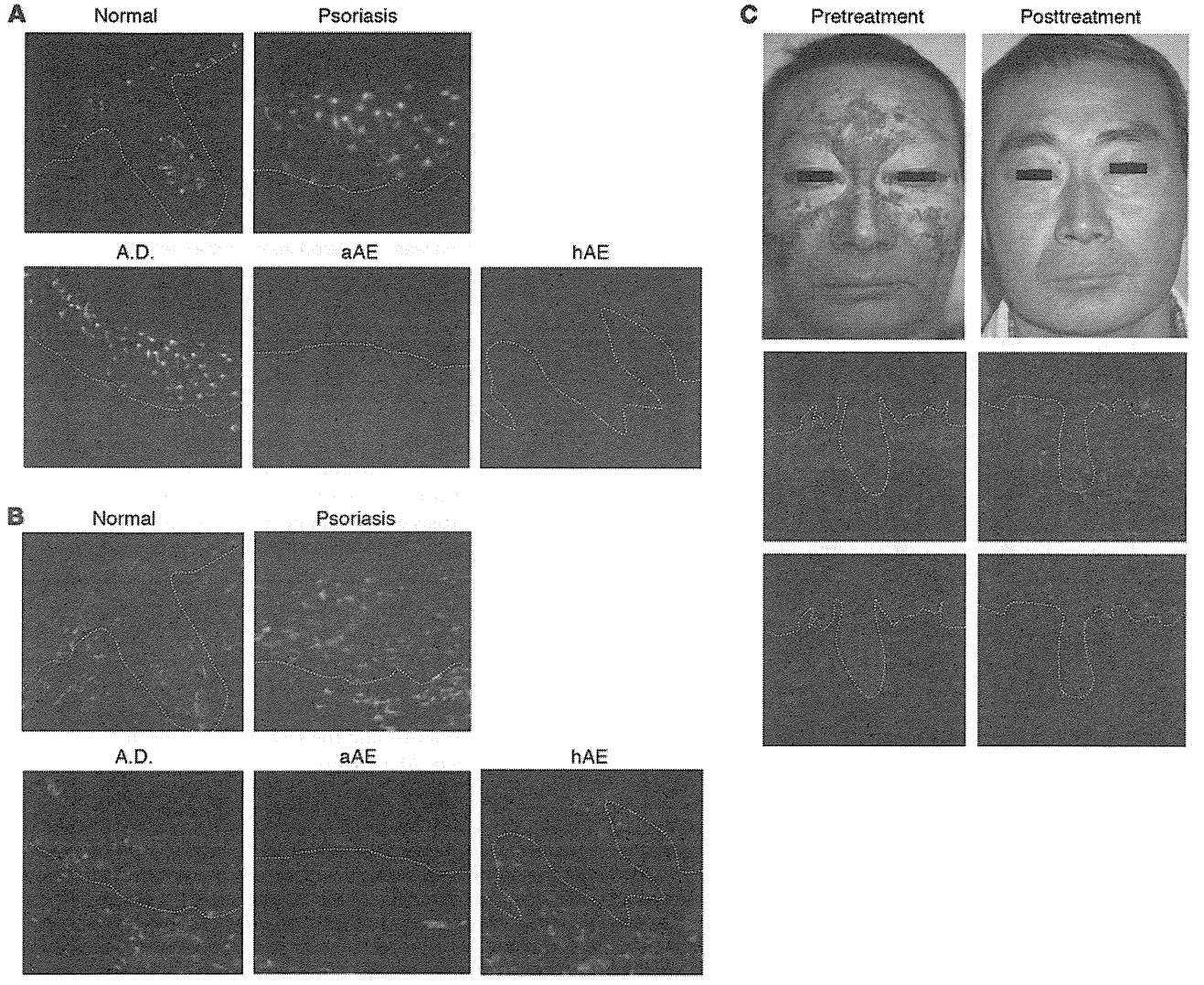

Figure 5
Loss of epidermal LCs in patients with AE. (**A** and **B**) Immunohistochemical staining for HLA-DR (green) and langerin (red) in the erythematous lesions of patients with psoriasis vulgaris (psoriasis), atopic dermatitis (A.D.), hereditary AE (hAE), and acquired AE (aAE) or normal skin. Original magnification, ×200. (**C**) Clinical appearance and immunohistochemical staining of a patient with hereditary AE before and after treatment by oral Zn supplement. White dotted lines denote the epidermis/dermis interface. Original magnification, ×200.

obtained from ZD mice were found to mediate significantly less SEAP activity than those from ZA mice (Figure 6C). In addition, we found that *Tgfb1* mRNA levels in epidermal sheets from ZD mice were significantly lower than those from ZA mice (Figure 6D). These results suggest that Zn deficiency decreases epidermal TGF-β1 expression in the steady state, and this might, at least in part, be associated with the reduction of epidermal LCs in Zn deficiency.

Because recent studies have shown that TGF-β1 has antiapoptosis effects in LCs or DCs (38, 39), we next assessed for apoptosis in epidermal LCs freshly isolated from ZA and ZD mice. As shown in Supplemental Figure 7A, the incidence of annexin V^+ cells in LCs from mice fed ZD diets for 3 weeks was slightly, but significantly, higher than that from mice fed ZA diets. We next performed in vitro experiments to obtain additional evidence for the hypothesis that Zn deficiency directly induces apoptosis of LCs. After in vitro culture of epidermal cell suspensions obtained from ZA mice with varying concentrations of TPEN for 48 hours, 5 μM TPEN significantly increased the incidence of annexin V^+ LCs (Supplemental Figure 7B). Similarly, we also found a significant increase of apoptosis in human monocyte-derived LCs cultured with TPEN at a concentration of 5 μM (Supplemental Figure 7C). Notably, consistent with a previous finding in HaCaT keratinocytes (40), Pam-212 keratinocytes cultured with 5 μM TPEN for 48 hours demonstrated no changes in cell viability and growth (data not shown). These results suggest that, in addition to the reduced TGF-β1 in epidermis, severe Zn deficiency may directly induce apoptosis in LCs, resulting in the loss of LC networks in ZD mice.

Enhanced ICD in the absence of LCs. At present, there are 2 types of LC ablation murine models. The first LC ablation model uses transgenic langerin$^-$ diphtheria toxin A (DTA) mice (41), which constitutively lack LCs. The second uses mice that express EGFP fused with a diphtheria toxin receptor (DTR) under the control

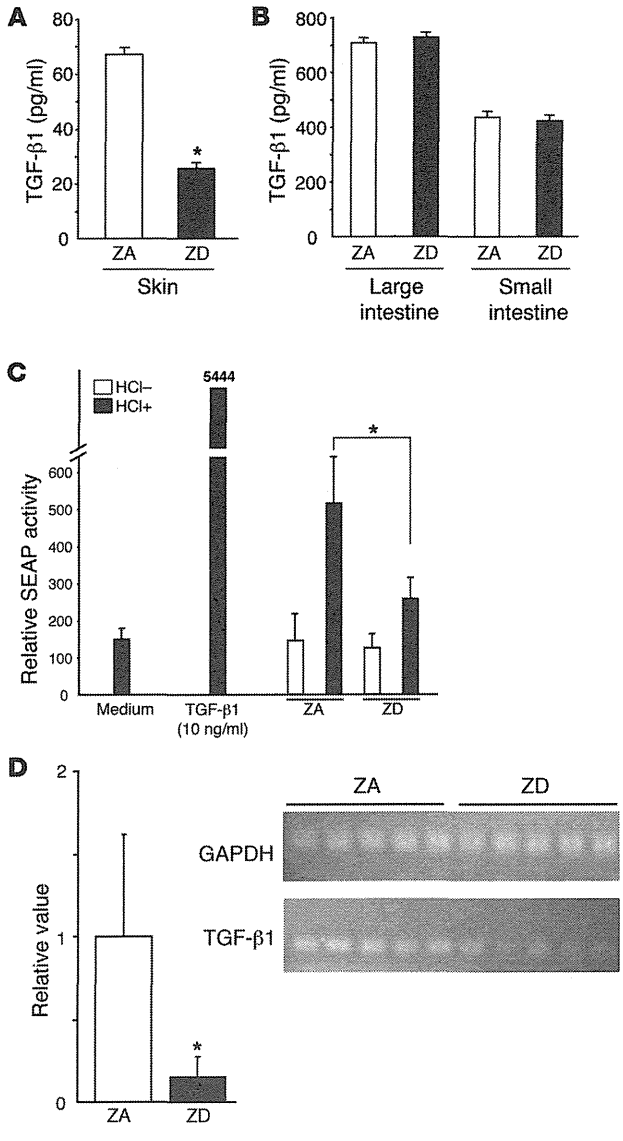

Figure 6

Decreased TGF-β1 production in the skin of ZD mice. (**A** and **B**) Samples of (**A**) skin tissue or (**B**) mucosal tissue were taken from the backs of mice fed a ZA (white bars) or ZD (black bars) diet for 5 weeks and cultured for 24 hours (n = 5). TGF-β1 secretion in the ex vivo skin or mucosa organ cultures was assessed by ELISA assays. (**C**) SEAP activity of the skin samples measured using MFB-F11 cells with or without HCl in the culture system. (**D**) Quantitative real-time RT-PCR for the detection of *Tgfb1* and *Gapdh* mRNAs in epidermis from the ears of mice fed a ZA (white bar) or ZD (black bar) diet for 5 weeks. The fold induction was calculated from normalized mRNA expression by the epidermis of ZD mice relative to that of ZA mice. Results are the mean ± SD (n = 5). *P < 0.05, compared with mice fed the ZA diet. Data are representative of several experiments with similar results.

of the langerin promoter, which are known as langerin-EGFP-DTR mice (42) and langerin-DTR mice (43). After i.p. injection of diphtheria toxin (DT) into langerin-EGFP-DTR mice, LCs do not repopulate for at least 4 weeks, while the number of langerin$^+$ dermal DCs in the skin recover to the basal level about 7 days after depletion by DT (44). Langerin-EGFP-DTR mice 14 days after treatment with DT are used as a model to deplete LCs alone. Fourteen days after treatment with DT, langerin-DTR mice and C57BL/6 (B6) mice were treated with 5%, 1%, and 0.5% CrO on the ears and monitored for ear swelling. As expected, the ear swelling response to 1% and 0.5% CrO in langerin-DTR mice was significantly increased at 12 and 24 hours after application compared with that in corresponding B6 mice (Figure 7). These results suggest that depletion of LCs enhances ICD responses, consistent with our findings that ZD mice lacking epidermal LCs exhibited increased ICD responses to 1% CrO (Figures 1 and 4).

Discussion

Although the skin is commonly involved and is often one of the first organs affected in Zn deficiency, the underlying pathophysiology of the inflammatory skin manifestation in AE remains unclear. Nearly pathognomonic in the histopathologic examination of AE is the presence of "necrolysis," a term describing cytoplasmic pallor, vacuolization, ballooning degeneration, and subsequent confluent necrosis of keratinocytes within the epidermis (8). As several in vitro studies have shown that Zn deficiency can induce cell death in HaCaT keratinocytes via apoptosis or necrosis (40, 45, 46), one of the mechanisms of epithelial damage observed in AE lesions might be by increased death of keratinocytes. However, the characteristic inflammatory dermatitis in clinical AE is seen only in the acral areas, suggesting the participation of additional cellular processes, which could account for the restricted localization of the dermatitis and the severe cutaneous inflammation in immunodeficient AE patients.

Our data, which we believe to be novel, reveal that irritants, but not haptens, can cause severe skin inflammation in immunodeficient ZD mice, providing a biologic basis for understanding the pathogenesis of AE. We found that ICD responses in ZD mice exhibited similar histological features similar to those of the characteristic dermatitis in clinical AE, highlighting the possibility that the acral, periorificial, and anogenital dermatitis in AE might be caused by contact with different irritants in daily life, such as chemicals, foods, urine, and feces, etc. We have addressed the mechanisms responsible for the severe and prolonged ICD in ZD mice and have identified several abnormalities which we believe to be novel, including aberrant chemokine gene expression and ATP release by keratinocytes in response to irritant chemicals. These 2 abnormalities are closely associated, because extracellular ATP induces keratinocyte *Cxcl1* and *Cxcl2* gene expression, major chemoattractants for neutrophils (Figure 3D and refs. 33, 34). Together with the insight that neutrophils are the pathogenic cells in ICD (31), our results suggest that ATP plays a key role in the pathogenesis of severe and prolonged ICD in Zn deficiency. This notion is supported by the finding that local injection of apyrase significantly diminished the ICD response in ZD mice (Figure 2E). Our in vitro assay revealed that membrane channel–mediated diffusible mechanisms play a pivotal role in the Zn deficiency–induced increased ATP release from irritant-stimulated keratinocytes (Supplemental Figure 3). However, because chemical irritants also trigger ATP release from keratinocytes as a consequence of cell damage or acute cell death (26, 28), Zn deficiency and irritants may synergistically induce keratinocyte cell damage, as shown in Figure 1B, leading to increased ATP release in vivo.

We found that ex vivo ATP release from CrO-treated skin was increased in Zn deficiency (Figure 2A). This observation is in line

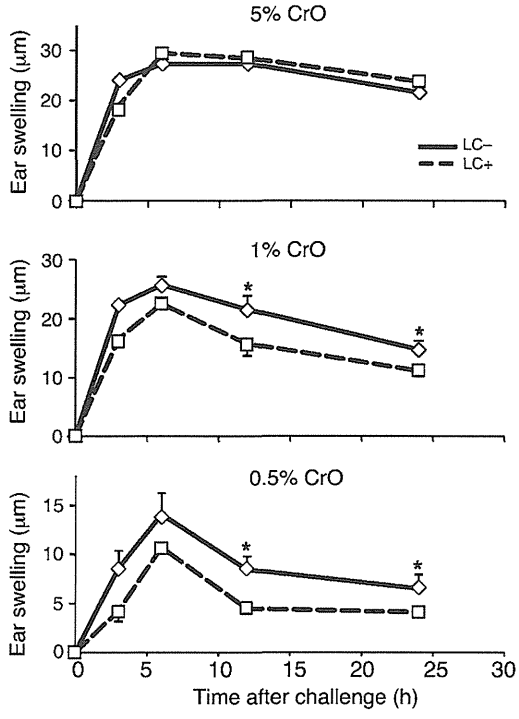

Figure 7
Enhanced ICD in the absence of LCs. Fourteen days after treatment with DT, langerin-DTR (LC–) and B6 (LC+) mice were applied with 5% (mean ± standard error [SE]; n = 4 and 6, respectively), 1% (mean ± SE; n =10 and 16, respectively), and 0.5% (mean ± SE; n = 6 and 10, respectively) CrO on the ears and monitored for ear swelling 3, 6, 12, and 24 hours later. Data are presented as the mean ± SEM (μm) and are a representative of 3 independent experiments. *P < 0.05, between langerin-DTR and corresponding B6 mice.

with our in vitro findings that Zn deficiency augments the release of ATP from irritant-stimulated Pam-212 keratinocytes. In addition, the decreased number of epidermal LCs observed in ZD mice (Figure 4) might also contribute to the increased ATP release from skin organ cultures ex vivo (Figure 2A) as well as the severe and prolonged ICD responses in vivo (Figure 1). Mechanisms include loss of the potent ecto-NTPDase activity of LC-associated CD39, which plays a protective role against ATP-mediated inflammation in ICD responses (28). Taken together, our results suggest that the inflammatory skin manifestations in patients with AE may occur as a result of excessive ICD responses, presumably due to aberrant ATP release upon repeated exposure to various irritants in daily life.

According to our data, Zn deficiency decreases epidermal TGF-β1 expression and its activity in the steady state. While the signaling via TGF-β receptor has been well defined, the homeostatic regulation of TGF-β is largely obscure. So far, the best-characterized regulator (inducer) of TGF-β expression is TGF-β itself (47), and an autocrine production of TGF-β1 is generally required for the homeostasis of various cell types, including LCs (48). Therefore, signaling molecules downstream of TGF-β receptor, such as Smad proteins, are thought to be involved in the regulation of their TGF-β production. Since a number of Zn finger transcription factors (e.g., ZNF580) has been reported to be associated with TGF-β signaling (49), Zn deficiency might decrease the autocrine production of TGF-β1 in LCs and keratinocytes by multiple pathways via those transcription factors.

The present results indicate that Zn deficiency induced the loss of epidermal LCs. Since several lines of evidence have indicated that TGF-β1 governs LC homeostasis (36, 50), the reduced TGF-β1 in epidermis may be, at least in part, responsible for the LC disappearance. The other possible mechanism for LC depletion is apoptosis, because several studies have suggested that Zn is an important physiological regulator of apoptosis (51). Indeed, the incidence of apoptosis in epidermal LCs in ZD mice was increased in the steady state (Supplemental Figure 7A). We also found that murine and human LCs underwent apoptosis when cultured with TPEN at a concentration of 5 μM (Supplemental Figure 7, B and C), while the culture condition did not induce apoptosis in keratinocytes (data not shown), suggesting that LCs are more sensitive to Zn deficiency-induced apoptosis. Taken together with the findings that TGF-β1 has antiapoptosis effects (38, 39), our results suggest that severe Zn deficiency may induce apoptosis in LCs through synergy between its direct effect and the reduced TGF-β1 expression, resulting in the loss of LC networks. Additional studies are needed to determine the impact of TGF-β1 on LC survival in vivo and the paramount mechanism underlying LC disappearance in ZD mice and patients with AE.

A previous study has reported that, in transgenic langerin-DTA mice, depletion of LCs does not affect ICD responses induced by 0.5%–2.5% sodium dodecyl sulfate or 5% BAC (41). In our study using langerin-EGFP-DTR mice, however, the ear swelling response to 1% and 0.5% CrO was significantly increased (Figure 7), consistent with the previous findings that LC-associated CD39 plays a protective role against ATP-mediated inflammation in ICD (28). Nevertheless, both langerin-DTR mice and control mice developed a similar degree of ear swelling after application of 5% CrO (Figure 7), as previously observed in transgenic langerin-DTA mice (41). Since CrO induces ATP release from keratinocytes in a dose-dependent manner (Figure 2), it is possible that an excess ATP release in ICD in response to a high dose of CrO in vivo might be beyond the capacity of NTPDase-dependent hydrolysis by LCs. Alternatively, differences in irritants or depletion timing might explain the phenotypic differences among the LC ablation models (41, 42). Further detailed analysis under different conditions is needed to reveal the functions and significance of LCs in ICD.

Methods

Animals and diet. Five-week-old female BALB/c mice were purchased from Oriental Yeast Co. Ltd. Mice were maintained under specific pathogen-free conditions throughout this study. ZD diet was purchased from CLEA Japan Inc. The mice were fed a powdered ZD diet or control diet from 5 to 11 weeks of age (n = 5–10 per group). Both diets were of almost the same nutritional quality, differing only in terms of Zn content (Zn, 0.11–0.38 mg/100 g in ZD diet, 6.00 mg/100 g in control diet). Langerin-EGFP-DTR mice on a B6 background (provided by Bernard Malissen, Université de la Méditerranée, Aix-en-Provence, Gap and Marseille, France) express a high-affinity human DTR in the langerin locus, as described previously (44). After i.p. injection of 1,000 ng DT in PBS, LCs do not repopulate for at least 4 weeks, while the number of langerin$^+$ dermal DCs in the skin recovers to the basal level about 7 days after depletion by DT (44).

Patients. Biopsies were obtained from lesional skin of patients, including those with atopic dermatitis, psoriasis vulgaris, hereditary AE (pretreatment and posttreatment with oral Zn sulfate), and acquired AE. Addition-

ally, control biopsies were obtained from healthy volunteers. The samples were snap frozen in liquid nitrogen and stored at -80°C.

Reagents and antibodies. DNFB, CrO, BAC, EPP, TPEN, CBX, and BAPTA-AM were purchased from Sigma-Aldrich. $ZnSO_4$ was purchased from Kanto Chemical Inc. FITC-conjugated anti-human HLA-DR, anti-mouse I-A^d, and CD90 (Thy-1) mAbs and PE-conjugated anti-mouse CD11c and I-A^d mAbs were purchased from BD Biosciences. Purified and PE-conjugated anti-human langerin mAbs were purchased from Abcam and R&D Systems, respectively.

ACD and ICD responses. For the induction of chemically induced allergic skin inflammation, mice were topically treated with 20 μl 0.5% DNFB dissolved in acetone/olive oil (4:1), which was painted onto the shaved abdomen at days 0 and 1. The ears were then challenged with 10 μl of 0.2% DNFB on the right ear and vehicle alone on the left ear on day 5. For chemically induced irritant skin inflammation, mice received topical application of 1% CrO, 10% BAC, or 30% EPP on the right ear and vehicle alone on the left ear. Swelling responses were quantified (right ear thickness minus left ear thickness) by a third experimenter using a micrometer, as described previously (28). In some experiments, potato apyrase grade VII (0.2 U/ear; Sigma-Aldrich) was injected s.c. into the ear 10 minutes before and 1 hour after CrO painting (28). In experiments with langerin-EGFP-DTR mice, 5%, 1% and 0.5% CrO was painted on the ears.

Quantification of ATP release from the skin and keratinocytes. ATP secretion from skin organ culture was quantified, as previously reported (52). Skin samples were taken from both ears immediately. s.c. fat was removed with a scalpel, and the skin explants were prepared by being cut into 8.0-mm circular pieces. The 2 pieces of skin from the 2 ears were floated with the epidermis side upward in 12-well plates containing 4 ml PBS and incubated on ice for 10 minutes. In some experiments, Pam-212 keratinocytes cultured in DMEM medium containing 10% FCS, 10 mM HEPES, 0.25 μg/ml gentamicin, and 2 mM L-glutamine were pretreated with 2 μM TPEN for 6 hours and then cultured with PBS with CrO, BAC, or EPP. ATP concentrations in the supernatants were then quantified using the luciferin-luciferase assay.

Preparation of epidermal cell suspensions and epidermal sheets. The ears were removed, mechanically divided into dorsal and ventral cutaneous sheets, and then incubated with a 0.5% solution of trypsin (type XI, Sigma-Aldrich) in PBS for 30 minutes at 37°C to separate the epidermis from the underlying dermis. After removal of the loosened dermis, the epidermal sheets were gently agitated with 0.05% DNase (DN25; Sigma-Aldrich) in PBS for 10 minutes, and the resulting EC suspension was passed through a nylon mesh to remove hair and stratum corneum prior to use. The viability determined by trypan blue exclusion was always more than 90% (53). For immunohistological staining, epidermal sheets were prepared from ear skin by incubation in 0.5 M ammonium thiocyanate (37°C for 20 minutes), fixed in acetone (-20°C for 30 minutes), and rehydrated in PBS (36).

Preparation of monocyte-derived LCs. Monocyte-derived LCs were cultured from PBMCs, as described previously (54). Briefly, monocytes were isolated by depletion of magnetically labeled nonmonocytes (Monocyte Isolation Kit II; Miltenyi Biotec) from plastic-adherent PBMCs obtained from healthy blood donors. Monocytes were cultured with 1,000 U/ml recombinant human GM-CSF (R&D Systems), 1,000 U/ml recombinant human IL-4 (R&D Systems), and 10 ng/ml human platelet-derived TGF-β1 (R&D Systems) for 7 days.

Flow cytometry. Single-cell suspensions (5×10^5) of epidermal sheets, inguinal and axillary lymph nodes, and spleens obtained from ZA and ZD mice (5 mice per group) were stained for LCs with FITC-conjugated anti-I-A^d and PE-conjugated anti-CD11c mAbs or for DETCs with FITC-conjugated anti-Thy-1 mAb for 30 minutes at 4°C. Live/dead discrimination was performed using propidium iodide (Sigma-Aldrich). After washing, samples were analyzed on a FACSCalibur (BD Biosciences). Annexin V-FITC and propidium iodide staining was carried out according to the instructions of BD Pharmingen.

Histological examination. Tissue specimens from the ears from ZA or ZD mice were surgically removed immediately after determination of ear swelling, embedded in OCT compound (Tissue-tek), frozen in liquid nitrogen, and stored at -80°C until use. Cryostat sections were fixed in absolute acetone and stained with H&E. For immunohistochemical staining, murine epidermal sheets were stained for LCs and DETCs with PE-conjugated anti-I-A^d mAb or FITC-conjugated anti-Thy-1 mAb, washed, and analyzed by fluorescence microscopy. For human skin samples, cryostat sections were double stained with FITC-conjugated anti-HLA-DR and PE-conjugated anti-langerin mAbs, washed, and analyzed by fluorescence microscopy. For formalin-fixed skin samples, they were stained with anti-HLA-DR and anti-langerin mAbs, incubated with biotinylated goat anti-mouse immunoglobulins, and then incubated with streptavidin-peroxidase. Reactions were developed with aminoethylcarbazole. Sections were incubated with a DAKO LSAB Kit, HRP (DakoCytomation) and then counterstained with Mayer's hematoxylin. Positive (HLA-DR and langerin) cells were counted at high magnification (×400) in 4 different fields, and the average number of positive cells per field was calculated for each sample.

DNA microarray analysis. RNA was harvested using TRIzol (Invitrogen) from epidermal sheets obtained from ZA and ZD mice 24 hours after vehicle or CrO exposure. Preparation of cRNA and hybridization of probe arrays (U133.2.plus) was performed according to the manufacturer's instructions (Affymetrix). Data were analyzed according to the MIAME rule. The average μ and SD σ values of ZA and ZD mouse distributions are (-0.049, 1.35) and (-0.041, 1.34), respectively. The accession numbers for each chemokine gene are as follows (GenBank; http://www.ncbi.nlm.nih.gov/genbank): AF065933.1 (*CCL2*), AF128218.1 (*CCL4*), AF128196.1 (*CCL9*), U50712.1 (*CCL12*), NM_011332.1 (*CCL17*), AF099052.1 (*CCL20*), NM_009138.1 (*CCL25*), NM_020279.1 (*CCL28*), NM_008176.1 (*CXCL1*), NM_009140.1 (*CXCL2*), NM_009141.1 (*CXCL5*), NM_008599.1 (*CXCL9*), NM_021274.1 (*CXCL10*), and AF252873.1 (*CXCL14*).

Quantitative real-time PCR analysis. Murine epidermal sheets were homogenized in liquid nitrogen using a Mikro-Dismembrator U (Braun Biotech). Total RNA was extracted from Pam-212 keratinocytes or homogenized epidermis using ISOGEN (Nippon Gene), and cDNA was synthesized using the SuperScript system (Invitrogen Life Technologies). Subsequently, relative mRNA expression was determined by real-time PCR using an ABI PRISM 5500 Sequence Detection System (Applied Biosystems) with SYBR Green I Dye (Qiagen). Primers corresponding to mouse chemokines, TGF-β, and G3PDH were designed by TAKARA BIO INC. Ct numbers were derived from the exponential phase of PCR amplification. Fold differences in the expression of gene x in the cell populations y and z were derived by the formula 2^k, where $k = (Ctx - CtG3PDH)y - (Ctx - CtG3PDH)z$.

Measurement of TGF-β production and its activity in mucosa and skin. To measure TGF-β production, skin and mucosa samples were taken from the trunk and the large or small intestine of ZA and ZD mice. The pieces of cutaneous (1.0 × 1.0 cm^2) or mucosal (100 mg) tissues were cultured with the epithelial side upward in 24-well plates containing 2 ml RPMI medium (Invitrogen), with 10% FCS, 10 mM HEPES, 0.25 μg/ml gentamicin, and 2 mM L-glutamine for 24 hours. TGF-β production in culture supernatants was measured by ELISA (R&D Systems). In general, TGF-β is secreted in a latent complex in which TGF-β homodimers are noncovalently associated with homodimers of the propeptide called the latency-associated peptide (LAP), and the release of TGF-β from its LAP is required for binding of TGF-β to the cellular receptors (55). To determine TGF-β activity, we used a bioassay using MFB-F11 cells stably transfected with the reporter plasmid containing 12 CAGA boxes (Smad-binding element) fused to a SEAP

reporter gene (56). Briefly, MFB-F11 cells (4×10^4 cells/well) in 96-well flat-bottom tissue culture plates were incubated in 50 μl serum-free DMEM for 2 hours, and then skin culture supernatants or TGF-β (10 pg/ml) were added in a 50 μl volume in the presence or absence of 10 μM HTS466284. After 24 hours of incubation, SEAP activity in the culture supernatants was measured using Gene Light 55 (Microtec).

Statistics. Significant differences between experimental groups were analyzed by Student's *t* test (1 tailed). *P* values less than 0.05 were considered significant.

Study approval. The murine studies were conducted with the approval of and in accordance with the Guidelines for Animal Experiments of the University of Yamanashi. The human study protocol was approved by the institutional review boards of the University Hospital (University of Yamanashi), and informed consent was obtained from all subjects.

Acknowledgments

We thank Takamitsu Matsuzawa, Rui Aoki, Miyuki Ogino, and Kayoko Ohshimo for technical assistance and Kazutoshi Harada and Naotaka Shibagaki for helpful discussions. We thank Akashi Izumi and Shigeo Ihara for their help with microarray analysis. These studies were supported in part by a grant from the Ministry of Education and Science of the Japanese Government.

Received for publication April 20, 2011, and accepted in revised form November 16, 2011.

Address correspondence to: Tatsuyoshi Kawamura, 1110 Shimokato, Chuo, Yamanashi 409-3898, Japan. Phone: 81.55.273.6766; Fax: 81.55.273.6766; E-mail: tkawa@yamanashi.ac.jp.

1. Prasad AS. Zinc: an overview. *Nutrition.* 1995; 11(1 suppl):93–99.
2. Vallee BL, Auld DS. Cocatalytic zinc motifs in enzyme catalysis. *Proc Natl Acad Sci U S A.* 1993; 90(7):2715–2718.
3. Brown KH, Peerson JM, Rivera J, Allen LH. Effect of supplemental zinc on the growth and serum zinc concentrations of prepubertal children: a meta-analysis of randomized controlled trials. *Am J Clin Nutr.* 2002;75(6):1062–1071.
4. Kitamura H, et al. Toll-like receptor-mediated regulation of zinc homeostasis influences dendritic cell function. *Nat Immunol.* 2006;7(9):971–977.
5. Yamasaki S, et al. Zinc is a novel intracellular second messenger. *J Cell Biol.* 2007;177(4):637–645.
6. Haase H, et al. Zinc signals are essential for lipopolysaccharide-induced signal transduction in monocytes. *J Immunol.* 2008;181(9):6491–6502.
7. Kabu K, et al. Zinc is required for Fc epsilon RI-mediated mast cell activation. *J Immunol.* 2006; 177(2):1296–1305.
8. Maverakis E, et al. Acrodermatitis enteropathica and an overview of zinc metabolism. *J Am Acad Dermatol.* 2007;56(1):116–124.
9. Kury S, et al. Identification of SLC39A4, a gene involved in acrodermatitis enteropathica. *Nat Genet.* 2002;31(3):239–240.
10. Wang K, Zhou B, Kuo YM, Zemansky J, Gitschier J. A novel member of a zinc transporter family is defective in acrodermatitis enteropathica. *Am J Hum Genet.* 2002;71(1):66–73.
11. Kury S, et al. Mutation spectrum of human SLC39A4 in a panel of patients with acrodermatitis enteropathica. *Hum Mutat.* 2003;22(4):337–338.
12. Maggini S, Wenzlaff S, Hornig D. Essential role of vitamin C and zinc in child immunity and health. *J Int Med Res.* 2010;38(2):386–414.
13. Song Y, et al. Dietary zinc restriction and repletion affects DNA integrity in healthy men. *Am J Clin Nutr.* 2009;90(2):321–328.
14. Rink L, Haase H. Zinc homeostasis and immunity. *Trends Immunol.* 2007;28(1):1–4.
15. Murakami M, Hirano T. Intracellular zinc homeostasis and zinc signaling. *Cancer Sci.* 2008; 99(8):1515–1522.
16. Shankar AH, Prasad AS. Zinc and immune function: the biological basis of altered resistance to infection. *Am J Clin Nutr.* 1998;68(2 suppl):447S–463S.
17. Prasad AS. Effects of zinc deficiency on Th1 and Th2 cytokine shifts. *J Infect Dis.* 2000; 182(suppl 1):S62–S68.
18. Prasad AS, et al. Serum thymulin in human zinc deficiency. *J Clin Invest.* 1988;82(4):1202–1210.
19. Richter M, Cantin AM, Beaulieu C, Cloutier A, Larivee P. Zinc chelators inhibit eotaxin, RANTES, and MCP-1 production in stimulated human airway epithelium and fibroblasts. *Am J Physiol Lung Cell Mol Physiol.* 2003;285(3):L719–L729.
20. Zhou Z, Wang L, Song Z, Saari JT, McClain CJ, Kang YJ. Abrogation of nuclear factor-kappaB activation is involved in zinc inhibition of lipopolysaccharide-induced tumor necrosis factor-alpha production and liver injury. *Am J Pathol.* 2004;164(5):1547–1556.
21. von Bulow V, et al. Zinc-dependent suppression of TNF-alpha production is mediated by protein kinase A-induced inhibition of Raf-1, I kappa B kinase beta, and NF-kappa B. *J Immunol.* 2007;179(6):4180–4186.
22. von Bulow V, Rink L, Haase H. Zinc-mediated inhibition of cyclic nucleotide phosphodiesterase activity and expression suppresses TNF-alpha and IL-1 beta production in monocytes by elevation of guanosine 3′,5′-cyclic monophosphate. *J Immunol.* 2005;175(7):4697–4705.
23. King LE, Fraker PJ. Zinc deficiency in mice alters myelopoiesis and hematopoiesis. *J Nutr.* 2002; 132(11):3301–3307.
24. Fraker PJ, King LE, Laakko T, Vollmer TL. The dynamic link between the integrity of the immune system and zinc status. *J Nutr.* 2000;130(5S suppl):1399S–1406S.
25. Lazarowski ER, Boucher RC, Harden TK. Mechanisms of release of nucleotides and integration of their action as P2X- and P2Y-receptor activating molecules. *Mol Pharmacol.* 2003;64(4):785–795.
26. Mizumoto N, Mummert ME, Shalhevet D, Takashima A. Keratinocyte ATP release assay for testing skin-irritating potentials of structurally diverse chemicals. *J Invest Dermatol.* 2003;121(5):1066–1072.
27. Koizumi S, Fujishita K, Inoue K, Shigemoto-Mogami Y, Tsuda M. Ca2+ waves in keratinocytes are transmitted to sensory neurons: the involvement of extracellular ATP and P2Y2 receptor activation. *Biochem J.* 2004;380(pt 2):329–338.
28. Mizumoto N, et al. CD39 is the dominant Langerhans cell-associated ecto-NTPDase: modulatory roles in inflammation and immune responsiveness. *Nat Med.* 2002;8(4):358–365.
29. Koizumi S, Fujishita K, Inoue K. Regulation of cell-to-cell communication mediated by astrocytic ATP in the CNS. *Purinergic Signal.* 2005;1(3):211–217.
30. Grabbe S, Schwarz T. Immunoregulatory mechanisms involved in elicitation of allergic contact hypersensitivity. *Immunol Today.* 1998;19(1):37–44.
31. Zhang L, Tinkle SS. Chemical activation of innate and specific immunity in contact dermatitis. *J Invest Dermatol.* 2000;115(2):168–176.
32. Meller S, et al. Chemokine responses distinguish chemical-induced allergic from irritant skin inflammation: memory T cells make the difference. *J Allergy Clin Immunol.* 2007;119(6):1470–1480.
33. Olson TS, Ley K. Chemokines and chemokine receptors in leukocyte trafficking. *Am J Physiol Regul Integr Comp Physiol.* 2002;283(1):R7–R28.
34. Ohara H, et al. Gene expression profiling defines the role of ATP-exposed keratinocytes in skin inflammation. *J Dermatol Sci.* 2010;58(2):143–151.
35. Merad M, Ginhoux F, Collin M. Origin, homeostasis and function of Langerhans cells and other langerin-expressing dendritic cells. *Nat Rev Immunol.* 2008;8(12):935–947.
36. Borkowski TA, Letterio JJ, Farr AG, Udey MC. A role for endogenous transforming growth factor beta 1 in Langerhans cell biology: the skin of transforming growth factor beta 1 null mice is devoid of epidermal Langerhans cells. *J Exp Med.* 1996;184(6):2417–2422.
37. Tesseur I, Zou K, Berber E, Zhang H, Wyss-Coray T. Highly sensitive and specific bioassay for measuring bioactive TGF-beta. *BMC Cell Biol.* 2006;7:15.
38. Riedl E, Strobl H, Majdic O, Knapp W. TGF-beta 1 promotes in vitro generation of dendritic cells by protecting progenitor cells from apoptosis. *J Immunol.* 1997;158(4):1591–1597.
39. Ohtani T, et al. TGF-beta1 dampens the susceptibility of dendritic cells to environmental stimulation, leading to the requirement for danger signals for activation. *Immunology.* 2009;126(4):485–499.
40. Wilson D, Varigos G, Ackland ML. Apoptosis may underlie the pathology of zinc-deficient skin. *Immunol Cell Biol.* 2006;84(1):28–37.
41. Kaplan DH, Jenison MC, Saeland S, Shlomchik WD, Shlomchik MJ. Epidermal langerhans cell-deficient mice develop enhanced contact hypersensitivity. *Immunity.* 2005;23(6):611–620.
42. Kissenpfennig A, et al. Dynamics and function of Langerhans cells in vivo: dermal dendritic cells colonize lymph node areas distinct from slower migrating Langerhans cells. *Immunity.* 2005;22(5):643–654.
43. Bennett CL, et al. Inducible ablation of mouse Langerhans cells diminishes but fails to abrogate contact hypersensitivity. *J Cell Biol.* 2005;169(4):569–576.
44. Honda T, et al. Compensatory role of Langerhans cells and langerin-positive dermal dendritic cells in the sensitization phase of murine contact hypersensitivity. *J Allergy Clin Immunol.* 2010;125(5):1154–1156.
45. Chai F, Truong-Tran AQ, Evdokiou A, Young GP, Zalewski PD. Intracellular zinc depletion induces caspase activation and p21 Waf1/Cip1 cleavage in human epithelial cell lines. *J Infect Dis.* 2000; 182(suppl 1):S85–S92.
46. Kolenko V, et al. Dead or dying: necrosis versus apoptosis in caspase-deficient human renal cell carcinoma. *Cancer Res.* 1999;59(12):2838–2842.
47. Kim SJ, Jeang KT, Glick AB, Sporn MB, Roberts AB. Promoter sequences of the human transforming growth factor-beta 1 gene responsive to transforming growth factor-beta 1 autoinduction. *J Biol Chem.* 1989;264(12):7041–7045.
48. Kaplan DH, Li MO, Jenison MC, Shlomchik WD, Flavell RA, Shlomchik MJ. Autocrine/paracrine TGF-beta1 is required for the development of epidermal Langerhans cells. *J Exp Med.* 2007;204(11):2545–2552.
49. Luo Y, Hu W, Xu R, Hou B, Zhang L, Zhang W. ZNF580, a novel C2H2 zinc finger transcription factor, interacts with TGF-beta signal molecule SMAD2. *Cell Biol Int.* 2011;35(11):1153–1157.
50. Hacker C, et al. Transcriptional profiling identifies Id2 function in dendritic cell development. *Nat Immunol.* 2003;4(4):380–386.

51. Chai F, Truong-Tran AQ, Ho LH, Zalewski PD. Regulation of caspase activation and apoptosis by cellular zinc fluxes and zinc deprivation: A review. *Immunol Cell Biol.* 1999;77(3):272–278.
52. Denda M, Inoue K, Fuziwara S, Denda S. P2X purinergic receptor antagonist accelerates skin barrier repair and prevents epidermal hyperplasia induced by skin barrier disruption. *J Invest Dermatol.* 2002;119(5):1034–1040.
53. Kawamura T, Azuma M, Kayagaki N, Shimada S, Yagita H, Okumura K. Fas/Fas ligand-mediated apoptosis of murine Langerhans cells. *J Dermatol Sci.* 2000;22(2):96–101.
54. Ogawa Y, Kawamura T, Kimura T, Ito M, Blauvelt A, Shimada S. Gram-positive bacteria enhance HIV-1 susceptibility in Langerhans cells, but not in dendritic cells, via Toll-like receptor activation. *Blood.* 2009;113(21):5157–5166.
55. Schmierer B, Hill CS. TGFbeta-SMAD signal transduction: molecular specificity and functional flexibility. *Nat Rev Mol Cell Biol.* 2007;8(12):970–982.
56. Nakamura Y, et al. House dust mite allergen Der f 1 can induce the activation of latent TGF-beta via its protease activity. *FEBS Lett.* 2009;583(12):2088–2092.

Characterization of dsRNA-induced pancreatitis model reveals the regulatory role of *IFN regulatory factor 2* (*Irf2*) in *trypsinogen5* gene transcription

Hideki Hayashi[a], Tomoko Kohno[a], Kiyoshi Yasui[a], Hiroyuki Murota[b], Tohru Kimura[c], Gordon S. Duncan[d], Tomoki Nakashima[e], Kazuo Yamamoto[d], Ichiro Katayama[b], Yuhua Ma[a], Koon Jiew Chua[a], Takashi Suematsu[a], Isao Shimokawa[f], Shizuo Akira[g], Yoshinao Kubo[a], Tak Wah Mak[d,1], and Toshifumi Matsuyama[a,h,1]

[a]Division of Cytokine Signaling, Department of Molecular Biology and Immunology and [f]Department of Investigative Pathology, Nagasaki University Graduate School of Biomedical Science, Nagasaki 852-8523, Japan; Departments of [b]Dermatology and [c]Pathology, Graduate School of Medicine and [g]Department of Host Defense, Research Institute for Microbial Diseases, Osaka University, Osaka 565-0871, Japan; [d]Campbell Family Cancer Research Institute, Princess Margaret Hospital, Toronto, ON, Canada M5G 2M9; [e]Department of Cell Signaling, Tokyo Medical and Dental University, Tokyo 113-8549, Japan; and [h]Global Center of Excellence Program, Nagasaki University, Nagasaki 852-8523, Japan

Contributed by Tak Wah Mak, October 5, 2011 (sent for review September 8, 2011)

Mice deficient for *interferon regulatory factor* (*Irf*)*2* (*Irf2*$^{-/-}$ mice) exhibit immunological abnormalities and cannot survive lymphocytic choriomeningitis virus infection. The pancreas of these animals is highly inflamed, a phenotype replicated by treatment with poly(I:C), a synthetic double-stranded RNA. Trypsinogen5 mRNA was constitutively up-regulated about 1,000-fold in *Irf2*$^{-/-}$ mice compared with controls as assessed by quantitative RT-PCR. Further knockout of *IFNα/β receptor 1*(*Ifnar1*) abolished poly(I:C)-induced pancreatitis but had no effect on the constitutive up-regulation of *trypsinogen5* gene, indicating crucial type I IFN signaling to elicit the inflammation. Analysis of *Ifnar1*$^{-/-}$ mice confirmed type I IFN-dependent transcriptional activation of dsRNA-sensing pattern recognition receptor genes *MDA5*, *RIG-I*, and *TLR3*, which induced poly(I:C)-dependent cell death in acinar cells in the absence of IRF2. We speculate that Trypsin5, the *trypsinogen5* gene product, leaking from dead acinar cells triggers a chain reaction leading to lethal pancreatitis in *Irf2*$^{-/-}$ mice because it is resistant to a major endogenous trypsin inhibitor, Spink3.

TRIF | IPS-1 | Ca^{2+}-binding proteins | cathepsin B

Interferons (IFNs) are cytokines whose actions contribute to the first line of defense against infection. IFNs both render cells resistant to viral attack and regulate cell growth and differentiation (1). IFNs elicit their pleiotropic effects by regulating the expression of many IFN-stimulated genes (ISGs). IFNs themselves are controlled by IFN regulatory factors (IRFs) that also regulate the expression of ISGs. By binding to IFN-stimulated response elements (ISREs) in gene promoters, the nine known IRF family members (IRF1–9) govern the production of cytokines related to inflammation and immune responses.

When pattern recognition receptors (PRRs) such as Toll-like receptors (TLRs) and retinoic acid-inducible gene-I (RIG)-like receptors detect pathogen ligands, these receptors are activated (2) and transduce downstream signaling, activating IRFs and IFNs. Analyses using knockout (KO) mice deficient for various IRFs have revealed their physiological roles. For example, IRF2 functions mainly as a transcriptional repressor by competing for binding to ISREs with other IRFs, especially IRF9 and IRF1 (1).

Irf2-deficient (*Irf2*$^{-/-}$) mice spontaneously develop inflammatory skin disease as they age, and die within weeks from lymphocytic choriomeningitis virus (LCMV) infection (3). Ablation of *IFNα/β receptor 1* (*Ifnar1*) or *Irf9* ameliorates the skin inflammation of *Irf2*$^{-/-}$ mice, suggesting that IRF2 negatively regulates gene expression by antagonizing IRF9, which is activated by type I IFN (I-IFN) (4). However, the precise mechanisms underlying the phenotypes of *Irf2*$^{-/-}$ are not known. In this study, we found that poly(I:C) (pIC) mimicked LCMV-induced pancreatitis, and we have used double KO mice to explore the cause of death in pIC-treated *Irf2*$^{-/-}$ mice. Our results show that significant trypsinogen5 up-regulation in *Irf2*$^{-/-}$ mice together with I-IFN-dependent transcriptional activation of dsRNA-sensing PRRs were critical for the pIC-induced death.

Results and Discussion

***Irf2*$^{-/-}$ Mice Show IFN-Dependent Poly(I:C)-Induced Pancreatitis and IFN-Independent Secretory Dysfunction in Pancreatic Acinar Cells.** LCMV-infected *Irf2*$^{-/-}$ mice die within 4 wk postinfection (3), but all *Irf2*$^{-/-}$ mice challenged intraperitoneally with poly(I:C) (pIC-*Irf2*$^{-/-}$ mice) died within 1 wk (Fig. 1*A*). Severe acute pancreatitis was apparent in pIC-*Irf2*$^{-/-}$ mice, as shown by abundant TUNEL^{+} apoptotic cells (Fig. 1*B*). Even in the absence of pIC, however, some abnormalities were detected in *Irf2*$^{-/-}$ pancreas, as indicated by hematoxylin and eosin staining (Fig. 1*C*) and electron microscopy (Fig. 1*D*). A mild infiltration of inflammatory cells (particularly lymphocytes) was noted around *Irf2*$^{-/-}$ ductal cells, but this pancreatitis was not typical. The pancreatic acinar cells in untreated *Irf2*$^{-/-}$ mice were filled with eosinophilic secretory granules of heterogeneous size, whereas fewer eosinophilic granules of more uniform size were observed mainly in the apical region of WT acinar cells. Interestingly, treatment of *Irf2*$^{-/-}$ mice with the stable cholecystokinin (CCK) analog cerulein (5) did not cause acute pancreatitis, as assessed by electron microscopy and serum amylase levels (Fig. S1 *A* and *B*). Because mRNA expression of CCK receptors in *Irf2*$^{-/-}$ mice was normal (Fig. S1*C*), these results suggest that the secretory and/or vesicle transport systems in *Irf2*$^{-/-}$ mice are dysfunctional.

The mRNAs encoding the Ca^{2+}-binding proteins Anxa10, Ahsg, and S100-G involved in Ca^{2+}-dependent vesicle transport, sorting, and fusion processes were significantly up-regulated in *Irf2*$^{-/-}$ pancreas (Table S1). The secretory dysfunction observed in cerulein-treated *Irf2*$^{-/-}$ mice (6), which is due to an abnormal distribution pattern of normal levels of soluble *N*-ethylmaleimide-sensitive factor attachment protein receptors (SNAREs) (6), may be due to the abnormal expression of these Ca^{2+}-binding proteins in the absence of IRF2, because annexin family proteins are known to bind and regulate SNAREs (7).

Skin inflammation in *Irf2*$^{-/-}$ mice was rescued by abolishing IFN signaling (4). We asked whether the atypical pancreatitis in *Irf2*$^{-/-}$ mice could be similarly rescued by crossing the *Irf2*$^{-/-}$ mutants to *Ifnar1*-, *Irf1*-, or *Trif*-deficient mice (3, 8, 9) to gen-

Author contributions: H.H., T. Kohno, I.K., T.W.M., and T.M. designed research; H.H., T. Kohno, K. Yasui, H.M., T. Kimura, G.S.D., T.N., K. Yamamoto, Y.M., K.J.C., T.S., and T.M. performed research; T. Kimura, I.S., and S.A. contributed new reagents/analytic tools; Y.K. and T.W.M. analyzed data; and H.H. and T.M. wrote the paper.

The authors declare no conflict of interest.

Freely available online through the PNAS open access option.

[1]To whom correspondence may be addressed. E-mail: tmak@uhnres.utoronto.ca or tosim@nagasaki-u.ac.jp.

This article contains supporting information online at www.pnas.org/lookup/suppl/doi:10.1073/pnas.1116273108/-/DCSupplemental.

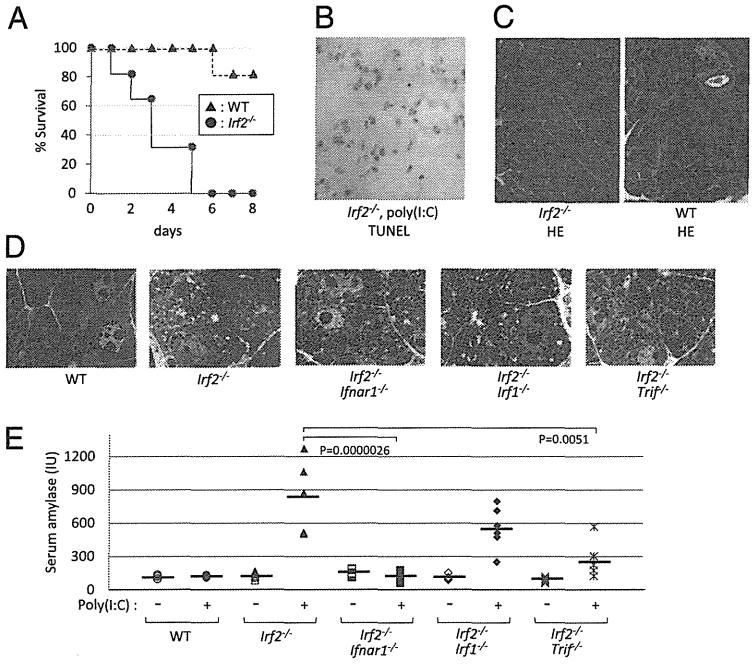

Fig. 1. *Irf2* deficiency induces sensitivity to poly(I:C) and pancreatitis. (*A*) Survival curve after pIC challenge. WT and *Irf2*-deficient ($Irf2^{-/-}$) mice were induced by i.p. pIC challenge (250 μg). All of the $Irf2^{-/-}$ mice were deceased within a week, compared with WT mice. (*B*) Following pIC stimulation, many cells were TUNEL-positive, indicating apoptosis and severe acute pancreatitis in $Irf2^{-/-}$ mice. (*C* and *D*) Hematoxylin and eosin (HE) staining (*C*) and electron microscopic observation (*D*) were done to examine the pancreas histologically in WT, $Irf2^{-/-}$, and double KO mice ($Irf2^{-/-}Ifnar1^{-/-}$, $Irf2^{-/-}Irf1^{-/-}$, and $Irf2^{-/-}Trif^{-/-}$). (*E*) To assess pancreatitis, we monitored serum amylase levels with (+) and without (–) pIC challenge.

erate double knockout mice. Abnormal acinar granule distribution was again observed in $Irf2^{-/-}Ifnar1^{-/-}$, $Irf2^{-/-}Irf1^{-/-}$, and $Irf2^{-/-}Trif^{-/-}$ mice (Fig. 1*D*). Thus, the abnormal acinar structure caused by *Irf2* disruption is not mediated by IFN signaling.

To assess pancreatitis in double knockout mice, we measured serum amylase levels before and after pIC challenge (Fig. 1*E*). Serum amylase was elevated in pIC-$Irf2^{-/-}$ and pIC-$Irf2^{-/-}Irf1^{-/-}$ mice. However, this increase did not occur at all in pIC-$Irf2^{-/-}Ifnar1^{-/-}$ mice, and only to a limited extent in pIC-IRF2$^{-/-}$TRIF$^{-/-}$ mice. These data indicate that type I IFN signaling via IFNAR1, as well as TLR signaling via the adaptor protein TRIF, are important for the development of pIC-induced pancreatitis in $Irf2^{-/-}$ mice. Moreover, our results show that IRF2 regulates IFN-independent pathways affecting acinar cell secretion as well as IFN-dependent pathways inducing pIC-mediated pancreatitis.

Up-Regulated Trypsinogen5 mRNA in the Pancreas of $Irf2^{-/-}$ Mice. We used an Affymetrix DNA microarray system to compare mRNA expression in the pancreas before and after pIC injection of $Irf2^{-/-}$ and WT mice (Fig. 2*A*). In $Irf2^{-/-}$ mice, 14 annotated genes were up-regulated and 8 genes were down-regulated more than 10-fold (Table S1) compared with WT mice. The transcriptional profiles of genes important for the etiology of pancreatitis (10, 11) are listed in Table 1. Strikingly, trypsinogen5 mRNA was up-regulated >100-fold in pIC-$Irf2^{-/-}$ pancreas, a noteworthy observation because trypsinogens activate many other pancreatic enzymes, and premature intracellular activation of trypsinogens in pancreatic acinar cells triggers acute pancreatitis (10, 11). There are 20 *trypsinogen* genes (*T1–T20*) in the murine T-cell receptor β gene locus (12), 12 of which express trypsinogen proteins (Fig. S2, *Right*), whereas humans have only 3 *trypsinogen* genes encoding three proteins: PRSS1, PRSS2, and PRSS3 (Fig. S2, *Left*) (13). The gene expression profile of pIC-$Irf2^{-/-}$ pancreas is inflammation-prone: Mouse trypsinogen mRNAs of T11 (Prss3) and T4 (Trypsinogen5) were up-regulated (Table 1); the mRNA encoding cysteine protease cathepsin B (Ctsb), an enzyme that can initiate pancreatitis by activating trypsinogens (14–16), was also up-regulated (Table 1). The mRNA encoding chymotrypsin C (Ctrc) was down-regulated and another anti-inflammatory factor inter-α-trypsin inhibitor was also down-regulated, although the mRNA encoding Kazal type 3 (Spink3), a serine protease inhibitor that blocks trypsin activity (17), was slightly up-regulated.

We examined the tissue specificity and dependency on IRF2 and IFNAR1 of trypsinogen5 expression by quantitative RT-PCR. In untreated WT mice, trypsinogen5 is expressed most highly in pancreas and skin and modestly in spleen (Fig. S3*A*). In untreated $Irf2^{-/-}$ mice, trypsinogen5 expression in the pancreas was up-regulated ~1,000-fold compared with controls, and was not affected by IFNAR1 ablation. Trypsinogen5 mRNA was up-regulated in $Irf2^{-/-}$ spleen to a much lower extent than in $Irf2^{-/-}$ pancreas, and was not detectable in liver or lung of WT or $Irf2^{-/-}$ mice.

We examined the effects of various IRFs on the activity of the murine *trypsinogen5* promoter, which contains seven ISREs. We cloned a 1.1-kb fragment of the *trypsinogen5* promoter region (−1063 to +15) to create a series of promoter deletion construct mutants driving the firefly luciferase reporter gene (Fig. 2*B*, *Left*). These were transfected into HEK293T cells along with plasmids overexpressing murine IRF1, human IRF5, IRF7, or MyD88. MyD88 was required for IRF-mediated activation of *trypsinogen5* ISREs, and significant promoter activity was observed when IRF1, IRF5, or IRF7 was overexpressed (Fig. S3*B*). Furthermore, the −216 to +15 promoter region of *trypsinogen5* was sufficient for responses to IRF1 or IRF7 stimulation (Fig. S3*C*). Overexpression of IRF2 inhibited IRF1- or IRF7-stimulated promoter activity in a dose-dependent manner (Fig. S3*D*). These data suggest that IRF2 binds to the proximal promoter of *trypsinogen5* and inhibits the access of IRF1, IRF5, and IRF7 to ISRE sites in this region.

To confirm this hypothesis, we transfected TGP49 cells, a mouse acinar cell line, with *trypsinogen5* promoter deletion series reporters as well as with plasmids expressing IRF1, -5, or -7, and assessed the promoter activities (Fig. 2*B*, *Right*). The basal promoter activity was drastically decreased by deleting the −216 to −100 region containing two ISREs, a nuclear factor-activated T cell (NFAT), and an activator protein 1 (AP-1) binding site. In contrast to 293T cells, the *trypsinogen5* promoter in TGP49 cells could be activated by exogenously expressed IRF5 or IRF7 without MyD88 (Fig. 3*A*). The promoter could not be activated by IRF1 even in the presence of MyD88 expression. The regions responsive to IRF5 and IRF7 were confirmed to be ISRE4 (−62 to −59) and ISRE3 (−55 to −49) by site-specific mutation analysis (Fig. 2*C*). The IRF5- and IRF7-dependent promoter activities were significantly ($P < 0.05$) enhanced by knocking down Irf2 with specific siRNA compared with control (scrambled) siRNA (Fig. 3*A*).

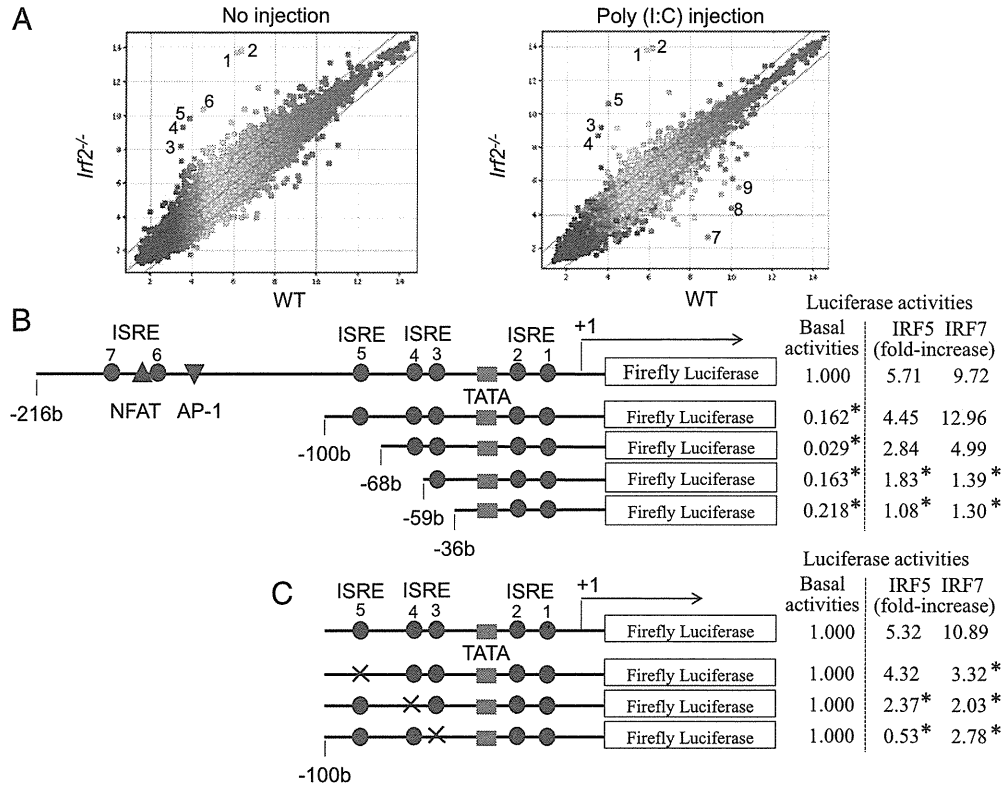

Fig. 2. Trypsinogen5 is highly expressed in *Irf2*-deficent mice. (*A*) *Irf2*$^{-/-}$ or wild-type mice with or without peritoneal injection of pIC were killed, and the amounts of mRNA from the pancreas were systematically compared using Affymetrix 28,815 gene probes. The points farthest from the diagonal indicate transcripts showing the greatest difference between WT and *Irf2*$^{-/-}$. Points 1 and 2, trypsinogen5 with different probes; 3, α-2-HS-glycoprotein (Ahsg); 4, annexin A10 (Anxa10); 5, fetuin-β (Fetub); 6, 3-hydroxy-3-methylglutaryl-CoenzymeA synthase2 (Hmgcs2, HMG-CoA synthase); 7, Ig κ chain variable8 (Igk-V8); 8, unknown; 9, carbonic anhydrase 3 (Car3). (*B*) A series of deletion mutants of *trypsinogen5* proximal promoter region (−216 to +15) was placed upstream of a luciferase reporter gene (1 μg) and analyzed for transcriptional activity in mouse pancreatic acinar cells using a dual luciferase assay at 24 h posttransfection in combination with expression vectors (100 ng) expressing IRF5 or IRF7 or a control vector. The basal luciferase activity of each deletion, measured relative to the −216 to +15 region, and the responses to IRF5 and IRF7 expression vectors are shown as fold increase compared with the control vector. The TATA box, ISRE core, and NFAT- and AP-1 binding sites are indicated. *$P < 0.05$ versus the −216 to +15 region. (*C*) Point mutations were introduced into each ISRE site (indicated by x) of the *trypsinogen5* promoters as described in *Materials and Methods*. The promoter activity of each mutant *trypsinogen5* was determined with a dual luciferase assay system. *$P < 0.05$ versus wild type.

To confirm IRF2 binding to the proximal promoter of trypsinogen5 in pancreatic acinar cells in vivo, we performed chromatin immunoprecipitation (ChIP) assays in TGP49 cells using specific PCR probes spanning all seven ISREs (−173 to +56) in the *trypsinogen5* promoter. Anti-IRF2 antibody specifically precipitated the *trypsinogen5* promoter, as determined by semi-quantitative PCR (Fig. 3*B*) and real-time PCR (Fig. 3*C*). These results suggest that in WT mice, trypsinogen5 expression in pancreatic acinar cells is repressed by the binding of IRF2 to ISREs in the proximal promoter region. However, in *Irf2*$^{-/-}$ mice, the *trypsinogen5* gene is activated because IRF5 and IRF7 can access the ISREs in the absence of IRF2.

IRF5 and IRF7 are critical inducers of the expression of proinflammatory cytokines and type I IFNs, respectively (18, 19), and these activities require MyD88. In WT cells, IRF4 inhibits IRF5 function by sequestering MyD88 (18). IRF2 did not associate with MyD88 (18) but, in our study, it did bind to the ISRE-containing region in the trypsinogen5 promoter (Fig. 3 *B* and *C*). Therefore, we postulate that IRF2 inhibits IRF5 and IRF7 activity by competing with them for binding to ISREs, rather than by sequestering MyD88.

Trypsinogen5 Is Resistant to the Trypsin Inhibitor Spink3. Comparison of mouse trypsinogen5 to other mouse and human trypsinogens (Fig. S4) showed that, although the N-terminal activation peptide sequence (NSDDK-I) in trypsinogen5 differs from that in other trypsinogens (DDDDK-I), other important regions, including the triad amino acid sequence H-D-S, required for enzymatic activity are conserved (10, 11). In addition, tryptic activity in cell lysates of 293FT cells overexpressing trypsinogen5 was dramatically enhanced by treatment with enteropeptidase (Fig. 4 *A* and *B*). The trypsinogen5 inhibitor binding site (DSCDGDS), which prevents premature activation, differed from that found in most trypsinogens (DSCQGDS) (10, 11), resembling the inhibitor binding site (DSCQRDS) of the human trypsin inhibitor-resistant PRSS3 enzyme. In addition, the trypsin autolytic cleavage site (Q-V) in trypsinogen5 differed from that in other trypsinogens (R-V), suggesting that trypsinogen5 is resistant to both trypsin inhibitors and self-inactivation. Indeed, trypsinogen5 was resistant to inhibition by Spink3, a major en-

Table 1. Expressions of relevant genes to pancreatitis

Gene transcripts	WT (−)	WT (pIC)	*Irf2*$^{-/-}$ (−)	*Irf2*$^{-/-}$ (pIC)
Prss1 (T16, Trypsin1)	11,161	13,863	10,388	13,788
Prss2 (T20, Trypsin 2)	16,041	15,661	15,857	15,494
Prss3 (T11, Trypsin 3)	1,155	1,131	3,059 ↑	2,395 ↑
Trypsinogen5 (T4, 1810009J06Rik)	70	57	13,514 ↑	14,287 ↑
Chymotrypsin C (Ctrc)	545	368	87 ↓	119 ↓
Chymotrypsinogen B 1 (Ctrb1)	19,417	18,772	20,457	19,919
Amylase2-2, pancreatic (Amy2b)	19,101	18,488	17,092	18,261
Calcium-sensing receptor (Casr)	37	37	30	26
Cystic fibrosis membrane conductance regulator (Cftr)	7	6	11	8
Cathepsin B (Ctsb)	349	443	848 ↑	794 ↑
Serine protease inhibitor, Kazal-type 3 (Spink3)	4,716	3,957	7,497	7,774
Inter-α-trypsin inhibitor, heavy chain 4 (Itih4)	375	212	78 ↓	71 ↓
Galanin (Gal)	879	1,057	213 ↓	71 ↓

The levels of gene expression in the pancreas are shown in Affymetrix units. The trypsinogen5 data are Point 1 in Fig. 2.

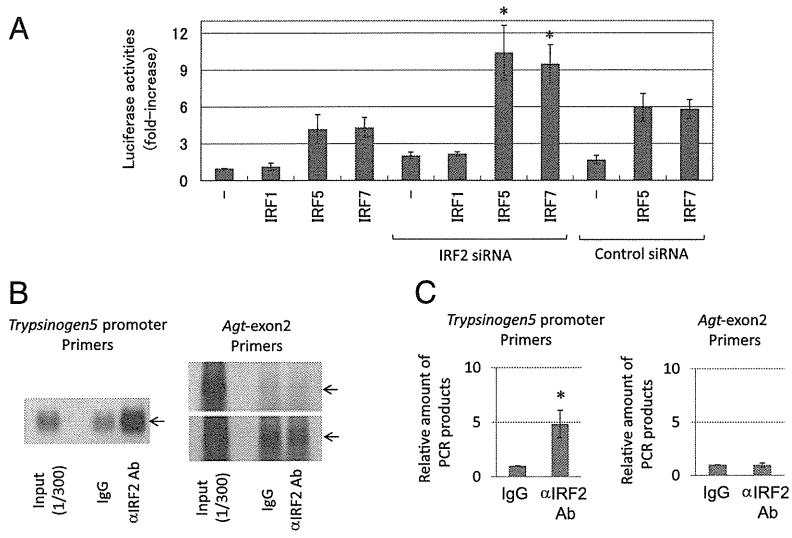

Fig. 3. IRF2 binds to the promoter region of *trypsinogen5* gene. (*A*) The effects of siRNAs (3 μg) specific to IRF2 or a control scrambled sequence on transcriptional activity of the −216 to +15 luciferase reporter in TGP49 acinar cells were measured. $*P < 0.05$ versus control siRNA. (*B*) A chromatin immunoprecipitation assay was done using TGP49 acinar cells with the IRF2-specific antibody (5 μg) or the same amount of control nonspecific IgG. The precipitated chromatin fragments were detected by PCR with a *trypsinogen5* promoter-specific primer set at 35 cycles or a negative control primer set for *angiotensinogen* (*Agt*) exon2 at 30 (*Upper*) and 35 (*Lower*) cycles. The input before precipitation indicates the predicted size (Trp5, 229 bp; Agt, 221 bp) of the PCR product. (*C*) The ChIP assay done in *B* was quantitatively measured using a real-time PCR method with the same primers. The relative amounts of β-actin were calculated, and the amounts of chromatin fragments precipitated with the anti-IRF2 antibody were shown relative to those with the nonspecific control antibody (IgG). $*P < 0.01$ versus control IgG.

dogenous trypsin inhibitor in mice (Fig. 4 *C* and *D*), as well as by soy bean trypsin inhibitor (Fig. S5 *A* and *B*). Analysis of the evolutionary pedigree in Fig. S6 showed that mouse trypsinogen5 is most distant from mPrss1 and mPrss2, just as human PRSS3 is most distant from PRSS1 and PRSS2. Therefore, we believe that mouse trypsinogen5 is a homolog of human PRSS3. Moreover, our data suggest that, in the absence of IRF2, trypsinogen5 is highly expressed and exacerbates pIC-induced pancreatitis due to its inhibitor-resistant nature.

Poly(I:C)-Induced Cell Death Can Be Triggered by a TLR3/TRIF-Dependent Pathway or a RIG-I/MDA5/IPS-1-Dependent Pathway. Although trypsinogen5 was up-regulated in untreated IRF2$^{-/-}$ mice, only mild inflammation around acinar cells was observed and pancreatitis did not occur. We hypothesize that trypsinogen5 as well as mPrss1, -2, and -3 leaking from dying acinar cells are activated by proteases such as cathepsin B or enteropeptidase, also released from these cells. These activated trypsins trigger signals to induce the death of many acinar cells, a process of cell death amplification we refer to as the "enhancing loop" of acinar cell death. In this way, the initial death of a few cells induced by pIC can precipitate severe pancreatitis. This idea is supported by a report that the extracellular or intracellular treatment of pancreatic acinar cells with active trypsins causes acinar cell death (20). In this study, the enteropeptidase cleavage site (-DDDDK-) of rat trypsinogen was replaced with a cleavage site (-RTKR-) recognized by paired basic amino acid-cleaving enzyme (PACE). This allowed the rat trypsinogen to be activated intracellularly with the ubiquitously expressed PACE enzyme rather than with enteropeptidase, which is expressed mainly in the duodenum. We created a PACE-trypsinogen5 enzyme that successfully induced the apoptosis of 293FT cells when overexpressed (Fig. 4 *E* and *F*). These results indicate that proteolytic activation of trypsinogen5 is sufficient to induce cell death.

Because pIC-dependent pancreatitis in *Irf2*$^{-/-}$ mice can be prevented by inactivating IFNAR1 signaling (Fig. 1*E*), we focused on IFN signaling pathways to identify candidates that might trigger initial cell death following pIC treatment. Indeed,

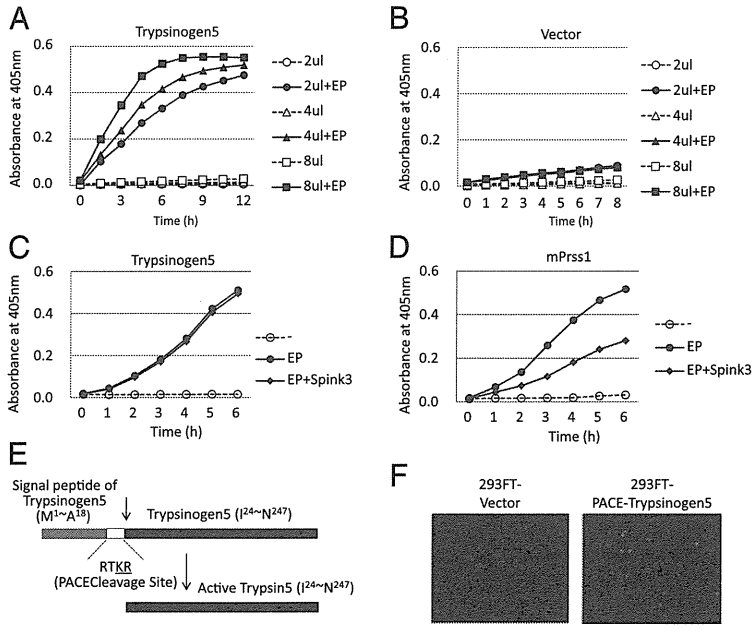

Fig. 4. Trypsinogen activity is activated by proteolytic cleavage. (*A* and *B*) A full-length mouse trypsinogen5 cDNA from the mouse pancreas was cloned into pcDNA3 (Invitrogen) and expressed in 293T cells. The indicated amounts of cell lysates (2–8 μL of 5 μg/μL lysates) were mixed with a trypsin-specific substrate (BioVision) in the presence or absence of added enteropeptidase. Tryptic activity was monitored by the amount of released pNA, measuring spectrophotometric units (A_{405}). (*C* and *D*) The effects of Spink3 were examined by adding cell lysates expressing Spink3, a major intrinsic trypsin inhibitor in mouse pancreas, to lysates expressing trypsinogen5 (*C*) or mouse Prss1 (*D*). (*E*) The DNA sequence encoding the activation peptide in the trypsinogen5 expression vector was replaced with sequences encoding a PACE cleavage site (-RTKR-) so that tryptic activity is activated by ubiquitously expressed PACE protease. (*F*) 293FT cells transfected with PACE-trypsinogen5 or control vector were stained with FITC-labeled annexin V to detect apoptosis.

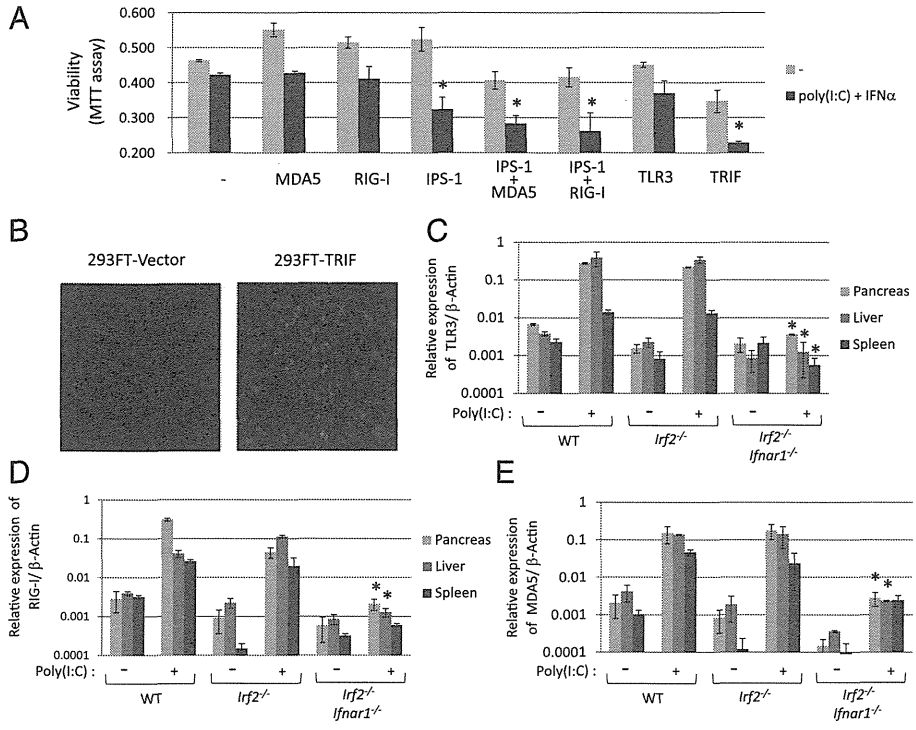

Fig. 5. Poly(I:C) and IFNα treatment induces cell death through different pathways. (*A*) Viabilities of 293FT cells transfected with the indicated expression plasmids in the presence or absence of pIC (5 μg/mL) and IFNα (50 ng/mL) for 44 h were quantified with the MTT assay. The values represent the average of at least three separate experiments, with SDs shown by error bars. TRIF and IPS-1 with MDA5 or RIG-I induced significant ($*P < 0.02$) cell death in response to pIC and IFNα. (*B*) 293FT cells transfected with TRIF expression vector or vector alone were stained with FITC-labeled annexin V to detect apoptosis. mRNA expression levels of TLR3 (*C*), RIG-I (*D*), and MDA5 (*E*) were measured using real-time PCR with (+) or without (–) i.p. pIC injection (250 μg). mRNAs prepared from pancreas, liver, and spleen of WT, *Irf2*$^{-/-}$, and *Irf2*$^{-/-}$*Ifnar1*$^{-/-}$ mice were converted into cDNA, and the amount of cDNA was determined by real-time PCR with the specific primers listed in *SI Materials and Methods*. The values represent the average of at least two mice, with SDs shown by error bars. $*P < 0.05$ versus *Irf2*$^{-/-}$ mice.

IRF1, *IRF7*, *MyD88*, *MDA5*, *RIG-I*, and *TLR3* gene expression were all up-regulated in the pancreas of pIC-*Irf2*$^{-/-}$ mice (Table S2). Because these proteins are associated with cell death pathways dependent on TRIF or IPS-1, we examined the effect of IRF2 loss on these well-characterized systems (21, 22). TRIF binds to receptor-interacting proteins and thereby activates caspase8 via FADD to induce cell death (21), whereas the IPS-1-dependent cell death pathway, which is triggered by MDA5 or RIG-I, is reported to activate caspase9 via the mitochondrial pathway dependent on Apaf-1 and cytochrome *c* (22). We confirmed that 293FT cells transfected with TRIF-expressing plasmid underwent apoptosis, as shown by staining with FITC-labeled annexin V (Fig. 5*B*). Next, we used the MTT viability assay to quantify the extent of cell death induced by IFN-related molecules in the presence or absence of pIC and IFNα. Exogenous overexpression of IPS-1 or TRIF significantly enhanced the death of pIC- and IFN-treated 293FT cells, and the death-inducing effects of MDA5 and RIG-I were enhanced by cotransfection with IPS-1 (Fig. 5*A*). These results suggest the existence of at least two pIC-dependent cell death pathways: one TLR3/TRIF-dependent and one RIG-I/MDA5/IPS-1-dependent.

We used real-time PCR to examine the induction of TLR3, RIG-I, and MDA5 mRNAs in pIC-treated WT, *Irf2*$^{-/-}$, and *Irf2*$^{-/-}$*Ifnar1*$^{-/-}$ mice. The levels of all three mRNAs were induced by nearly 100-fold in both pIC-WT and pIC-*Irf2*$^{-/-}$ mice, and these increases were abolished by deletion of IFNAR1 (Fig. 5 *C*–*E*). The IFN signal activation triggered by pIC is essential to initiate TLR3/TRIF- and RIG-I/MDA5/IPS-1-dependent acinar cell death, but is not sufficient to cause pancreatitis (Table S3). The elevation of trypsinogen5 expression mediated by abolishing IRF2 is also necessary for enhancing the cell death leading to lethal pancreatitis.

Activation Mechanisms of Mouse Trypsinogen5 and Human PRSS3. Trypsinogens (including trypsinogen5) can be activated in pancreatic acinar cells, or in other cells or tissues by enteropeptidase expressed in nonduodenal cells (23) such as in keratinocytes and oral carcinoma cells (24, 25). It is possible that keratinocyte-expressed enteropeptidase activates the trypsinogen5 expressed in skin (Fig. S3*A*), promoting age-dependent skin inflammation in *Irf2*$^{-/-}$ mice (4). Another possibility could be that proteases in addition to enteropeptidase can cleave pancreatic trypsinogen5. We have confirmed that cathepsin B, whose expression was elevated in *Irf2*$^{-/-}$ mice, can activate trypsinogen5 in vitro (Fig. S5*C*). The last possibility is that autocatalytic cleavage of trypsinogen, usually restricted under steady-state conditions, is accelerated in response to chemical stress or viral infection. Indeed, the autoactivation of trypsinogen is reportedly accelerated in low pH or by Ca^{2+} in vitro (26).

In conclusion, this study has identified important genes associated with IRF2 functions in mice. Our results suggest that IRF2 influences the expression of mouse trypsinogen5, whose human counterpart is PRSS3. Our data should therefore help to elucidate new IRF functions in humans.

Materials and Methods

Mice. *Irf1*$^{-/-}$ and *Irf2*$^{-/-}$ mice have been described (3). *IFNαIβ receptor 1* (*Ifnar1*)$^{-/-}$ mice were purchased from B&K Universal (8). TRIF$^{-/-}$ mice have been described (9). *Irf2*$^{-/-}$*Ifnar1*$^{-/-}$, *Irf2*$^{-/-}$*Irf1*$^{-/-}$, and *Irf2*$^{-/-}$*Trif*$^{-/-}$ double mutant mice were generated by crossing *Irf2*$^{+/-}$ with *Ifnar1*$^{-/-}$, *Irf1*$^{-/-}$, and *Trif*$^{-/-}$ mice, respectively. All mice were maintained under specific pathogen-free conditions and used at 6–12 wk of age. All experiments were performed according to institutional guidelines.

Cells. Human embryonic kidney (HEK)293T and 293FT (Invitrogen) cells and HeLa cells were cultured in DMEM supplemented with 10% FBS. Mouse pancreatic acinar TGP49 cells were cultured in a 1:1 mixture of DMEM and Ham's F-12 medium supplemented with 10% FBS.

Histological Analysis. Pancreas tissues were fixed overnight in 10% formalin, embedded in paraffin, sectioned, and stained with hematoxylin (0.4%) and eosin (0.5%) for light microscopic analysis. For electron microscopic analysis, the tissues were fixed in 2.5% glutaraldehyde solution buffered to pH 7.4 with 0.1 M phosphate buffer for 4 h at 4 °C. Postfixation was performed with 2% osmium tetroxide solution buffered to pH 7.4 with the same buffer for 2 h at 4 °C, and they were embedded, sectioned, and doubly stained with uranyl acetate and lead nitrate.

Microarrays. Total RNAs from the pancreas of wild-type and *Irf2*$^{-/-}$ mice aged 6 wk, harvested 3 h after no injection or a peritoneal injection with 250 μg poly(I:C), were used in the array studies. The quality of the RNA was assessed with an Agilent 2100 Bioanalyzer, and samples of 100 ng total RNA were reverse-transcribed and then amplified by in vitro transcription according to Affymetrix standard protocols. The mouse Affymetrix GeneChip Mouse Gene 1.0 ST Array was used in all hybridizations. These arrays contain probes representing transcripts for 28,815 mouse gene entities. Microarray data were analyzed using Affymetrix Expression Console software and Gene Spring GX, whereas differentially expressed genes were identified with annotation.

Real-Time RT-PCR. Total RNA was prepared from tissues using the acid phenol-guanidinium thiocyanate method after immersing the tissues for more than overnight in RNAlater Solution (Ambion). Reverse transcription was conducted for 60 min at 46 °C from 200 ng of purified total RNA using SuperScript III (Invitrogen), followed by 45 cycles of PCR (15-s denaturation at 95 °C, 25-s annealing at 55 °C, and 15-s extension at 72 °C). An SYBR Green PCR Kit (Qiagen) was used to monitor the PCR products on a LightCycler 1.5 and real-time PCR detection system (Roche). Primers designed for the respective genes are listed in *SI Materials and Methods*.

Plasmid Constructs. cDNAs encoding human IRF5, IRF7, and IPS-1 were generated from total RNA prepared from 293T cells by RT-PCR using KOD-FX DNA polymerase (Toyobo). Human MDA5, RIG-I, and TLR3 cDNAs were generated from total RNA prepared from THP-1 (a human leukemia cell line) or HeLa cells by RT-PCR. Mouse Trypsinogen5, Prss1, and Spink3 cDNAs were made from total RNA prepared from WT mouse pancreas by PCR. All constructs generated by PCR were confirmed by DNA sequencing. The p*Trypsinogen5*-Luc reporter plasmid was constructed by inserting the promoter region (−1063 to +15) of the mouse *trypsinogen5* gene by PCR into the pGL2-Basic vector. A series of deletion mutants was prepared using proper restriction enzymes (NcoI at −833; SpeI at −579; ScaI at −386; PvuII at −216) and a specific primer for the −100 site. The promoter region (−216 to +15) of the mouse *trypsinogen5* gene was used to introduce point mutations into the ISREs. The point mutations of ISRE3 (−55 to −49, ATTGAAA→GTTTGCG), ISRE4 (−62 to −59, TTTC→CGCA), and ISRE5 (−84 to −78, AATGAAA→GATTGCG) were introduced by overlap PCR mutagenesis. All constructs generated by PCR were confirmed by DNA sequencing.

PACE-Trypsinogen5 was constructed by replacing the activation peptide (-NSDDK-) of mouse trypsinogen5 cDNA with the PACE recognition peptide (-RTKR-) by overlap PCR mutagenesis.

Luciferase Reporter Assay. 293T cells (1×10^5 per well) were plated in 24-well plates and transfected 24 h later with 200 ng of the firefly luciferase reporter plasmid p*Trypsinogen5*-Luc, using FuGENE6 (Roche), along with each expression vector (20 ng unless otherwise stated) as indicated. In all cases, cells were transfected with 20 ng pRL-TK (*thymidine kinase* promoter-driven Renilla luciferase reporter gene; Promega) to normalize the transfection efficiency. TGP49 cells (1×10^5 per well) were plated in 12-well plates and transfected 24 h later with 1 μg of the firefly luciferase reporter plasmid pTrypsinogen5-Luc using Lipofectamine 2000 (Invitrogen), along with each expression vector (100 ng unless otherwise stated) as indicated. In all cases, cells were transfected with 20 ng pRL-RSV (RSV promoter-driven Renilla luciferase reporter gene). At 26 h posttransfection, luciferase activity was determined with a dual luciferase assay system (Promega). Mouse IRF2-specific and control siRNAs were purchased from Santa Cruz Biotechnology.

Chromatin Immunoprecipitation. Nuclear extracts from TGP49 cells were subjected to DNA–protein cross-linking with 1% formaldehyde for 5 min. After extensive washing, the samples were suspended in 500 μL of 150 mM NaCl, 25 mM Tris (pH 7.5), 5 mM EDTA, 1% Triton X-100, 0.1% SDS, and 0.5% deoxycholate and sonicated. After centrifugation at 14,000 rpm for 10 min at 4 °C, the supernatants were immunoprecipitated with 0.5 μg anti-IRF2 antibody, or the corresponding IgG (Sigma) (as a control), and Protein A Sepharose4B Fast Flow beads. The amounts of precipitated DNA were quantified by PCR using a pair of mouse *Trypsinogen5* promoter-specific primers and *Angiotensinogen* exon2-specific primers (*SI Materials and Methods*).

Trypsin Activity Assay. Trypsin activity was monitored by the amount of released *p*-nitroanilide (pNA) from a specific substrate, measuring spectrophotometric units at 405 nm (A_{405}) (Trypsin Activity Assay Kit; BioVision). Cell lysates prepared at 48 h posttransfection of the indicated expression plasmids were used with or without enteropeptidase (light chain, porcine; GenScript).

Cell Death Assay. Pancreatic tissues were used in a TUNEL assay. Briefly, tissue sections were incubated with 20 μg/mL proteinase K for 20 min, followed by inhibition of endogenous peroxidase by incubation with 2% H_2O_2 for 7 min. TdT (GIBCO-BRL) and biotinylated dUTP (Roche) in TdT buffer [0.1 M potassium cacodylate (pH 7.2), 2 mM $CoCl_2$, 0.2 mM DTT] were added to the sections and incubated in a humid atmosphere at 37 °C for 90 min after immersion in TdT buffer. The reaction was terminated by transferring the slides to TB buffer (300 mM NaCl, 30 mM Na citrate) for 30 min. The sections were covered with 10% rabbit serum for 10 min and then with the avidin–biotin peroxidase complex for 30 min. Finally, 3,3′-diaminobenzidine (DAB) was used as the chromogen. To detect apoptotic cells, FITC-conjugated annexin V (BioVision) was used according to the manufacturer's instruction. An MTT (ICN) assay to assess living cells was performed according to the manufacturer's instruction.

ACKNOWLEDGMENTS. This work was supported by Grants-in-Aid from the Ministry of Education, Culture, Sports, Science and Technology of Japan (22659092) and by the Global Center of Excellence Program at Nagasaki University.

1. Savitsky D, Tamura T, Yanai H, Taniguchi T (2010) Regulation of immunity and oncogenesis by the IRF transcription factor family. *Cancer Immunol Immunother* 59:489–510.
2. Kawai T, Akira S (2011) Toll-like receptors and their crosstalk with other innate receptors in infection and immunity. *Immunity* 34:637–650.
3. Matsuyama T, et al. (1993) Targeted disruption of IRF-1 or IRF-2 results in abnormal type I IFN gene induction and aberrant lymphocyte development. *Cell* 75:83–97.
4. Hida S, et al. (2000) CD8(+) T cell-mediated skin disease in mice lacking IRF-2, the transcriptional attenuator of interferon-α/β signaling. *Immunity* 13:643–655.
5. Lampel M, Kern H-F (1977) Acute interstitial pancreatitis in the rat induced by excessive doses of a pancreatic secretagogue. *Virchows Arch A Pathol Anat Histol* 373:97–117.
6. Mashima H, et al. (2011) Interferon regulatory factor-2 regulates exocytosis mechanisms mediated by SNAREs in pancreatic acinar cells. *Gastroenterology* 141:1102–1113.
7. Gerke V, Creutz C-E, Moss S-E (2005) Annexins: Linking Ca^{2+} signalling to membrane dynamics. *Nat Rev Mol Cell Biol* 6:449–461.
8. Hwang SY, et al. (1995) A null mutation in the gene encoding a type I interferon receptor component eliminates antiproliferative and antiviral responses to interferons α and β and alters macrophage responses. *Proc Natl Acad Sci USA* 92:11284–11288.
9. Yamamoto M, et al. (2003) Role of adaptor TRIF in the MyD88-independent Toll-like receptor signaling pathway. *Science* 301:640–643.
10. Chen J-M, Férec C (2009) Chronic pancreatitis: Genetics and pathogenesis. *Annu Rev Genomics Hum Genet* 10:63–87.
11. Whitcomb D-C (2010) Genetic aspects of pancreatitis. *Annu Rev Med* 61:413–424.
12. Spicuglia S, Pekowska A, Zacarias-Cabeza J, Ferrier P (2010) Epigenetic control of Tcrb gene rearrangement. *Semin Immunol* 22:330–336.
13. Rowen L, et al. (2005) Interchromosomal segmental duplications explain the unusual structure of PRSS3, the gene for an inhibitor-resistant trypsinogen. *Mol Biol Evol* 22:1712–1720.
14. Figarella C, Miszczuk-Jamska B, Barrett A-J (1988) Possible lysosomal activation of pancreatic zymogens. Activation of both human trypsinogens by cathepsin B and spontaneous acid. Activation of human trypsinogen 1. *Biol Chem Hoppe Seyler* 369 (Suppl):293–298.
15. Halangk W, et al. (2000) Role of cathepsin B in intracellular trypsinogen activation and the onset of acute pancreatitis. *J Clin Invest* 106:773–781.
16. Meister T, et al. (2010) Missorting of cathepsin B into the secretory compartment of CI-MPR/IGFII-deficient mice does not induce spontaneous trypsinogen activation but leads to enhanced trypsin activity during experimental pancreatitis—without affecting disease severity. *J Physiol Pharmacol* 61:565–575.
17. Hashimoto D, et al. (2008) Involvement of autophagy in trypsinogen activation within the pancreatic acinar cells. *J Cell Biol* 181:1065–1072.
18. Negishi H, et al. (2005) Negative regulation of Toll-like-receptor signaling by IRF-4. *Proc Natl Acad Sci USA* 102:15989–15994.
19. Honda K, et al. (2005) Spatiotemporal regulation of MyD88-IRF-7 signalling for robust type-I interferon induction. *Nature* 434:1035–1040.
20. Ji B, Gaiser S, Chen X, Ernst S-A, Logsdon C-D (2009) Intracellular trypsin induces pancreatic acinar cell death but not NF-&kappaB activation. *J Biol Chem* 284: 17488–17498.
21. Kaiser W-J, Offermann M-K (2005) Apoptosis induced by the Toll-like receptor adaptor TRIF is dependent on its receptor interacting protein homotypic interaction motif. *J Immunol* 174:4942–4952.
22. Lei Y, et al. (2009) MAVS-mediated apoptosis and its inhibition by viral proteins. *PLoS One* 4:e5466.
23. Yahagi N, et al. (1996) Complementary DNA cloning and sequencing of rat enteropeptidase and tissue distribution of its mRNA. *Biochem Biophys Res Commun* 219:806–812.
24. Nakanishi J, Yamamoto M, Koyama J, Sato J, Hibino T (2010) Keratinocytes synthesize enteropeptidase and multiple forms of trypsinogen during terminal differentiation. *J Invest Dermatol* 130:944–952.
25. Vilen S-T, et al. (2008) Intracellular co-localization of trypsin-2 and matrix metalloprotease-9: Possible proteolytic cascade of trypsin-2, MMP-9 and enterokinase in carcinoma. *Exp Cell Res* 314:914–926.
26. Chen J-M, et al. (2003) Evolution of trypsinogen activation peptides. *Mol Biol Evol* 20: 1767–1777.

2. Liu CH, Wu KH, Lin TY, Wei CC, Lin CY, Chen XX, et al. Wiskott-Aldrich syndrome with IgA nephropathy: a case report and literature review. Int Urol Nephrol 2012 [Epub ahead of print].
3. Matsukura H, Kanegane H, Miya K, Ohtsubo K, Higuchi A, Tanizawa T, et al. IgA nephropathy associated with X-linked thrombocytopenia. Am J Kidney Dis 2004; 43:e7-12.
4. Tomana M, Novak J, Julian BA, Matousovic K, Konecny K, Mestecky J. Circulating immune complexes in IgAN consist of IgA1 with galactose-deficient hinge region and antiglycan antibodies. J Clin Invest 1999;104:73-81.
5. Shimizu M, Nikolov NP, Ueno K, Ohta K, Siegel RM, Yachie A, et al. Development of IgA nephropathy-like glomerulonephritis associated with Wiskott–Aldrich syndrome protein deficiency. Clin Immunol 2012;142:160-6.
6. Lasseur C, Allen AC, Deminière C, Aparicio M, Feehally J, Combe C. Henoch-Schöenlein purpura with immunoglobulin A nephropathy and abnormal IgA in Wiskott-Aldrich syndrome carrier. Am J Kidney Dis 1997;29:285-7.
7. Moldoveanu Z, Wyatt RJ, Lee JY, Tomana M, Julian BA, Mestecky J, et al. Patients with IgA nephropathy have increased serum galactose-deficient IgA1 levels. Kidney Int 2007;71:1148-54.
8. Higgins EA, Siminovitch KA, Zhuang DL, Brockhausen I, Dennis JW. Aberrant O-linked oligosaccharide biosynthesis in lymphocytes and platelets from patients with the Wiskott-Aldrich syndrome. J Biol Chem 1991;266:6280-90.
9. Nguyen DD, Maillard MH, Cotta-de-Almeida V, Mizoguchiv E, Klein C, Fuss I, et al. Lymphocyte-dependent and Th2 cytokine-associated colitis in mice deficient in Wiskott-Aldrich syndrome protein. Gastroenterology 2007;133:1188-97.

Available online October 31, 2012.
http://dx.doi.org/10.1016/j.jaci.2012.08.040

Antigen-specific T-cell responses in patients with non–IgE-mediated gastrointestinal food allergy are predominantly skewed to T_H2

To the Editor:

IgE-mediated allergy is triggered by cross-linking of antigen-specific IgE antibodies on the cell surfaces of mast cells and basophils, followed by local accumulation and activation of inflammatory cells, including eosinophils and T_H2 cells. T_H2 cells produce such cytokines as IL-4, IL-5, and IL-13, which promote IgE production and eosinophilopoiesis and play central roles in the development of chronic allergic inflammation. On the other hand, non–IgE-mediated allergies, such as hypersensitivity pneumonitis, are considered mediated by cellular immunity, which has not been thought to involve antigen-specific T_H2 cells because IgE antibody would be detected if T_H2 cells were activated. Non–IgE-mediated gastrointestinal food allergies include food protein–induced enterocolitis syndrome (FPIES), food protein–induced proctocolitis, and food protein–induced enteropathy. The precise underlying mechanisms are almost unknown, except for a fundamental role of TNF-α,[1] presumably because this disease entity is relatively rare in incidence and is encountered during infancy in human subjects but not seen in experimental animals. Here, for the first time, we were able to detect antigen-specific T_H2 cell responses in infants with non–IgE-mediated gastrointestinal food allergies by analyzing 89 blood samples collected from all over Japan.

The antigen-specific lymphocyte stimulation test is a classic method for investigating antigen-specific T-cell proliferation and theoretically should be applicable to the study of gastrointestinal food allergies. However, a couple of previous studies demonstrated that the antigen-specific lymphocyte stimulation test was useful, whereas another study found no such usefulness.[2] We hypothesized that this controversy was due to contamination of the antigen preparations with LPS and tested this hypothesis. The limulus amebocyte lysate assay detected high concentrations of LPS in commercially available milk protein preparations, as previously reported (see Table E1 in this article's Online Repository at www.jacionline.org).[3] In addition, significant lymphoproliferative responses were found in the presence of as little as 10 pg/mL LPS (see Fig E1, *A*, in this article's Online Repository at www.jacionline.org), and PBMCs from younger children showed more pronounced lymphoproliferation in response to LPS (see Fig E1, *B*). Therefore we attempted to remove contaminating LPS from milk protein preparations by passing them through a prepacked endotoxin affinity column. However, a high LPS concentration was detected even after that treatment (see Table E1), and therefore we obtained a special β-lactoglobulin preparation with very low contaminating LPS levels (kindly provided by Bean Stalk Snow, Tokyo, Japan). Further studies were performed by using these milk protein preparations, which contained LPS at a final concentration of less than 5 pg/mL.

Next, to elucidate what types of antigen-specific immune responses are induced in patients with gastrointestinal food allergies, we cultured PBMCs from patients and control subjects in the presence and absence of LPS-depleted milk component proteins. The study enrolled 65 patients with gastrointestinal food allergies, 12 patients with IgE-mediated cow's milk allergy (CMA) who showed only nongastrointestinal symptoms on ingestion of milk, and 12 control subjects who showed absolutely no symptoms on ingestion of milk. Table I[4] summarizes the clinical symptoms, clinical diagnosis, and demographic data for the 2 patient groups. None of the patients with gastrointestinal food allergies had detectable levels of IgE against milk proteins in sera. We were unable to recruit infants with IgE-mediated CMA who were age matched with the infants with non–IgE-mediated

TABLE I. Demographic characteristics of the patients

	IgE-mediated CMA		Gastrointestinal food allergies	
	No.		No.	
Age (mo)	12	38.0 (26.5-60.0)	65	2.0 (1.0-4.0)
Male/female sex	12	7/5	65	40/25
Day of onset	12	—	65	32.5 (7.0-115.5)
Symptoms at onset				
Vomiting	12	0% (0/12)	65	53.8% (35/65)
Bloody stool	12	0% (0/12)	65	47.7% (31/65)
Diarrhea	12	0% (0/12)	65	47.7% (31/65)
Failure to thrive	12	0% (0/12)	65	38.4% (22/65)
Lethargy	12	0% (0/12)	65	38.4% (22/65)
Fever	12	0% (0/12)	65	18.5% (12/65)
Eczema	12	100% (12/12)	65	7.7% (5/65)
Wheeze	12	33.3% (3/12)	65	0% (0/65)
Laboratory data				
Milk-specific IgE (IU/mL)	12	56.95 (11.74-90.8)	65	<0.34 (<0.34)
Peripheral blood eosinophils (%)		Not examined	53	7.7 (3.6-13.5)

Data are expressed as medians (interquartile ranges). The inclusion criteria were as follows: (1) gastrointestinal symptoms were present more than 2 hours after ingestion of milk and (2) 3 of Powell's criteria were fulfilled,[4] including (a) switch to therapeutic milk leading to resolution of symptoms, (b) differential diagnosis from other disorders, and (c) verified body weight gain. A definitive diagnosis based on the results of oral food challenge tests that were performed after complete resolution of the initial symptoms was achieved in 19 patients. Patients with gastrointestinal symptoms within 2 hours after ingestion of milk were excluded. On the basis of such symptoms as vomiting, diarrhea, and failure to thrive, the patient group (n = 65) consists of 34 patients with FPIES, 4 patients with food protein–induced enteropathy syndrome (enteropathy), and 27 patients with food protein–induced proctocolitis syndrome (proctocolitis). A definitive diagnosis based on the results of oral food challenge tests was achieved in 13 and 6 patients with FPIES and proctocolitis, respectively. None of the patients underwent endoscopic biopsy.

TABLE II. Antigen-specific lymphoproliferation and cytokine production profiles in patients with gastrointestinal food allergies, patients with IgE-mediated allergy, and control subjects

	Control subjects		IgE-mediated CMA		Gastrointestinal food allergies			
	No.		No.		No.		*P* value†	*P* value‡
Proliferation (SI)*	20	1.290 (0.830-1.738)	9	3.077 (2.484-3.492)	65	2.894 (2.004-7.147)	<.01	<.001
Cytokine (pg/mL)								
TNF-α	12	74.69 (58.44-144.8)	10	77.78 (58.04-141.4)	65	241.0 (89.21-729.6)	NS	<.05
IL-6	12	79.24 (36.36-193.8)	10	337.9 (57.43-1021)	65	1151 (157.0-4802)	NS	<.01
IL-1β	11	26.02 (6.880-46.47)	10	27.49 (6.548-65.04)	64	48.75 (11.7-136.1)	NS	NS
IL-2	12	4.15 (0.0-10.04)	10	12.31 (7.23-17.58)	58	16.32 (7.760-39.49)	NS	<.01
IL-3	12	0.0 (0.0-0.38)	10	0.40 (0.0-3.61)	62	4.22 (0.0-29.49)	NS	<.05
IL-4§	12	5.365 (2.895-6.358)	10	3.795 (2.033-7.788)	65	5.670 (2.775-12.06)	NS	NS
IL-5	12	2.080 (0.0-19.56)	10	46.59 (4.663-173.5)	65	63.66 (7.360-310.4)	NS	<.01
IL-10	12	9.285 (3.075-15.71)	10	56.17 (18.74-76.91)	65	57.92 (12.61-198.8)	NS	<.05
IL-13	12	21.61 (0.270-65.04)	10	82.56 (16.28-555.3)	65	291.7 (22.10-1417)	NS	<.01
IFN-γ	11	3.910 (0.0-67.06)	10	31.91 (3.635-102.0)	65	71.86 (5.49-303.4)	NS	NS
IL-17	12	0.0 (0.0-2.350)	10	7.635 (1.710-39.63)	65	7.150 (0.0-17.83)	NS	NS

PBMCs from each patient were stimulated separately with each of 5 different milk protein preparations, and the data show the highest concentration of each cytokine detected in response to the 5 different stimuli. Data are expressed as medians (interquartile ranges).

*The stimulation index *(SI)* was calculated as milk protein–specific tritiated thymidine uptake (cpm)/vehicle-induced tritiated thymidine uptake (cpm).

†Nonparametric test to compare control subjects and patients with IgE-mediated CMA.

‡Nonparametric test to compare control subjects and patients with gastrointestinal food allergies.

§According to the standard curve, the minimal detection limit was 5.88 pg/mL.

gastrointestinal food allergies. This study was approved by regional ethics committees, and written informed consent was obtained from the guardians of all patients and control subjects.

The details of the lymphoproliferation test and cytokine production assay are described in the Methods section in this article's Online Repository at www.jacionline.org. In brief, PBMCs from heparinized peripheral blood were suspended at a cell density of 1×10^6/mL in AIM-V medium (Gibco, Grand Island, NY) without serum. Lymphoproliferation was measured by using tritiated thymidine uptake during a 16-hour period after a 5-day stimulation with 100 μg/mL of each LPS-depleted milk protein preparation (α-lactalbumin, β-lactoglobulin, and α-, β- and κ-caseins). PBMCs were suspended at 1×10^6/mL in RPMI 1640 medium supplemented with 5% autologous plasma to investigate the antigen-specific cytokine production profiles. Culture supernatants were harvested at day 6 after stimulation with 100 μg/mL of each LPS-depleted milk protein preparation, and the cytokine production profiles were investigated by using the Luminex multiplex cytokine analysis kits (Millipore, Bedford, Mass) and ELISA (R&D Systems, Minneapolis, Minn).

In the first series of experiments, we investigated milk protein–specific lymphoproliferation in the control subjects, patients with IgE-mediated CMA, and patients with gastrointestinal food allergies. The lymphoproliferation level was similar in the patients with IgE-mediated CMA and those with gastrointestinal food allergies. Unlike in previous studies, however, the control subjects showed almost no proliferation (Table II). We presume that this was due to the extensive depletion of LPS contaminating the antigen preparations and the use of serum-free medium.

In the next experiments we investigated the cytokine production profiles in these subjects. TNF-α concentrations in the culture supernatants of milk protein–stimulated PBMCs from patients with gastrointestinal food allergies were significantly greater than those seen in patients with IgE-mediated CMA or control subjects. However, TNF-α levels in supernatants from patients with IgE-mediated CMA and control subjects were similar (Table II). Significantly higher concentrations of another proinflammatory cytokine, IL-6, were also seen only in the patients with gastrointestinal food allergies.

The concentrations of 3 T_H2 cytokines, IL-3, IL-5, and IL-13, in the supernatants of milk protein–stimulated PBMCs from patients with IgE-mediated CMA tended to be higher than those in the control subjects, but the differences did not reach statistical significance. In contrast, statistically significant and much higher concentrations of these T_H2 cytokines were found for the patients with gastrointestinal food allergies. Another T_H2 cytokine, IL-4, was undetectable in almost all subjects, and there were no differences among the 3 groups.

Concentrations of the T_H1 cytokine IFN-γ and the T_H17 cytokine IL-17 did not show statistically significant differences between any 2 groups.

The milk component that caused the most prominent tritiated thymidine uptake or the most prominent IL-2 or TNF-α production varied among the patients (see Fig E3 in this article's Online Repository at www.jacionline.org), suggesting that the lymphoproliferation and cytokine production observed in these assays were indeed antigen specific. In addition, the IL-5 concentration in the culture supernatant of cow's milk protein–stimulated PBMCs from patients with gastrointestinal food allergies correlated significantly with the peripheral blood eosinophil ratio at disease onset (see Fig E4 in this article's Online Repository at www.jacionline.org), suggesting that our *in vitro* assay reflects the *in vivo* conditions in these patients.

Collectively, T_H2 cytokines, including IL-3, IL-5, and IL-13, but not the T_H1 cytokine IFN-γ or the T_H17 cytokine IL-17 were significantly produced *in vitro* by milk protein–stimulated PBMCs from patients with gastrointestinal food allergies. The findings that tritiated thymidine uptake correlated significantly with IL-13 production (data not shown) along with the absence of milk-specific IgE antibody strongly suggest that the IL-13 detected in our assay was not produced by basophils in the PBMC fraction. IL-13 is a well-established mediator of intestinal

epithelial cell damage in patients with injuries and inflammatory diseases through activation of the tumor necrosis factor-like weak inducer of apoptosis-fibroblast growth factor-inducible molecule 14 (TWEAK-Fn14) axis.[5] Thus in addition to the previously known TNF-α, IL-13 might play a crucial role in the pathogenesis of gastrointestinal food allergies.

In conclusion, antigen-specific T-cell responses in patients with non–IgE-mediated gastrointestinal food allergy are predominantly skewed to T_H2. It remains unclear why antigen-specific IgE antibodies were not detected in these patients. Possible explanations are that neonatal B cells scarcely express IL-4/IL-13 receptors[6] or that production of IgE antibodies had just started but was still undetectable. This question warrants further study.

We express our sincere gratitude to all the members of the Japanese Research Group for Neonatal Infantile Allergic Disorders. We also thank all the doctors, nurses, and technicians, especially Ms Nao Aida from the Division of Allergy, Gastroenterology, Pathology, Surgery, Interdisciplinary Medicine and Neonatology of the National Center for Child Health and Development, for their hard work and valuable comments. We also thank Professor Mitsuaki Kimura (Department of Allergy and Clinical Immunology, Shizuoka Children's Hospital) for his valuable suggestions.

Hideaki Morita, MD, PhD[a,b]
Ichiro Nomura, MD, PhD[a,c]
Kanami Orihara, PhD[a]
Koichi Yoshida, MD[c,d]
Akira Akasawa, MD, PhD[c,d]
Hiroshi Tachimoto, MD, PhD[e]
Yoshikazu Ohtsuka, MD, PhD[f]
Yoshiyuki Namai, MD[g]
Masaki Futamura, MD, PhD[c]
Tetsuo Shoda, MD[a,c]
Akio Matsuda, PhD[a]
Norio Kamemura, MSc[h]
Hiroshi Kido, MD, PhD[h]
Takao Takahashi, MD, PhD[b]
Yukihiro Ohya, MD, PhD[c]
Hirohisa Saito, MD, PhD[a]
Kenji Matsumoto, MD, PhD[a]

From [a]the Department of Allergy and Immunology, National Research Institute for Child Health and Development, Tokyo, Japan; [b]the Department of Pediatrics, Keio University School of Medicine, Tokyo, Japan; [c]the Division of Allergy, National Center for Child Health and Development, Tokyo, Japan; [d]the Department of Allergy, Tokyo Metropolitan Children's Medical Center, Tokyo, Japan; [e]the Department of Pediatrics, Jikei University School of Medicine, Tokyo, Japan; [f]the Department of Pediatrics and Adolescence Medicine, Juntendo University Graduate School of Medicine, Tokyo, Japan; [g]the Department of Pediatrics, Ohta Nishinouchi Hospital, Koriyama, Japan; and [h]the Division of Enzyme Chemistry, Institute for Enzyme Research, University of Tokushima, Tokushima, Japan. E-mail: nomura-i@ncchd.go.jp, matsumoto-k@ncchd.go.jp.

Supported in part by Health and Labour Sciences Research Grants, Research on Intractable Diseases from the Ministry of Health, Labour and Welfare, Japan, and a Grant-in-Aid for Clinical Research from the National Hospital Organization of Japan.

Disclosure of potential conflict of interest: I. Nomura has received support from the Ministry of Health, Labor, and Welfare. The rest of the authors declare that they have no relevant conflicts of interest.

REFERENCES

1. Chung HL, Hwang JB, Park JJ, Kim SG. Expression of transforming growth factor beta1, transforming growth factor type I and II receptors, and TNF-alpha in the mucosa of the small intestine in infants with food protein-induced enterocolitis syndrome. J Allergy Clin Immunol 2002;109:150-4.
2. Giavi S, Megremis S, Papadopoulos NG. Lymphocyte stimulation test for the diagnosis of non-IgE-mediated cow's milk allergy: a step closer to a noninvasive diagnostic tool? Int Arch Allergy Immunol 2012;157:1-2.
3. Brix S, Bovetto L, Fritsché R, Barkholt V, Frøkiaer H. Immunostimulatory potential of beta-lactoglobulin preparations: effects caused by endotoxin contamination. J Allergy Clin Immunol 2003;112:1216-22.
4. Powell GK. Food protein-induced enterocolitis of infancy: differential diagnosis and management. Compr Ther 1986;12:28-37.
5. Kawashima R, Kawamura YI, Oshio T, Son A, Yamazaki M, Hagiwara T, et al. Interleukin-13 damages intestinal mucosa via TWEAK and Fn14 in mice—a pathway associated with ulcerative colitis. Gastroenterology 2011;141:2119-29.
6. Tian C, Kron GK, Dischert KM, Higginbotham JN, Crowe JE Jr. Low expression of the interleukin (IL)-4 receptor alpha chain and reduced signalling via the IL-4 receptor complex in human neonatal B cells. Immunology 2006;119:54-62.

Available online October 16, 2012.
http://dx.doi.org/10.1016/j.jaci.2012.09.005

Forkhead box protein 3 (*FOXP3*) hypermethylation is associated with diesel exhaust exposure and risk for childhood asthma

To the Editor:

Traffic-related air pollutants, such as diesel exhaust particles (DEP), significantly contribute to the pathogenesis of wheezing and asthma in early childhood.[1] These illnesses are characterized by chronic airway inflammation caused by a dysregulated immune system.[2] Attention has recently been directed toward regulatory T (Treg) cells because they are important in suppressing immune responses against nonspecific stimuli,[3] such as DEP. The suppressive phenotype of Treg cells is conferred by stable expression of forkhead box protein 3 (*FOXP3*).[3] Transcriptional silencing of *FOXP3* through hypermethylation of CpG islands in the promoter and intronic regions has been identified as a hallmark of committed Treg cells and human diseases, including asthma.[3,4] As such, Nadeau et al[4] reported increased *FOXP3* hypermethylation in blood DNA to be associated with diminished Treg cell function and increased asthma severity in children exposed to polycyclic aromatic hydrocarbons, a component of DEP. In this study we test the novel hypothesis that early (birth) and consistent exposure to high levels of traffic pollution alters *FOXP3* methylation status in DNA from saliva in a manner that correlates with DEP exposure, predicts wheezing/asthma in later life, or both. The oral cavity provides an important first line of defense against DEP exposure for children because mouth breathing is a common path of exposure.[5] Furthermore, other aerodigestive track tissues, such as buccal cells, have been successful in characterizing DNA methylation with respect to air pollutants and airway inflammation.[6,7] The ancillary goal is to establish a noninvasive, high-throughput, and quantitative assay for measuring risk of asthma linked to traffic-related air pollution.

TABLE I. Distribution of *FOXP3* percentage methylation in the sample population stratified by respiratory outcomes

Description	Mean	Minimum	Maximum	SD
Study sample	21.30	0.00	62.40	17.40
Wheezing phenotype				
Nonwheezers	17.00	0.00	55.10	16.20
Persistent wheezers*	35.84	18.10	58.35	15.20
Early transient wheezers*	24.16	0.32	61.30	17.90
Asthma status				
Nonasthmatic	19.50	0.00	62.40	16.90
Asthmatic†	32.70	1.10	58.40	17.90

*Significant difference between persistent wheezers ($P < .01$) and early transient wheezers ($P < .05$) compared with nonwheezers.
†Significant difference between asthmatic and nonasthmatic children ($P < .05$).

METHODS

Heparinized blood samples were stored at room temperature and transferred to the National Research Institute for Child Health and Development in Tokyo. The following procedures were performed no later than 24 hours after phlebotomy. PBMCs were obtained from peripheral blood by using Ficoll-Hypaque gradient sedimentation (Lymphocyte Separation Medium; ICN Biochemicals, Aurora, Ohio). The viability determined by using trypan blue dye exclusion (Sigma, St Louis, Mo) always exceeded 95%. PBMCs were suspended at a cell density of 1×10^6/mL in AIM-V medium (Gibco) without serum for lymphoproliferation, and in RPMI 1640 medium (GIBCO/Life Technologies, Gaithersburg, Md) in the presence of 5% autologous plasma for cytokine production assays.

Lymphoproliferation was measured based on tritiated thymidine (Amersham, Tokyo, Japan) uptake during a 16-hour period after 5 days of stimulation with 100 μg/mL of each LPS-depleted milk protein preparation (α-lactalbumin, Sigma; β-lactoglobulin, Bean Stalk Snow; and α-, β-, and κ-caseins, Sigma) at 37°C in a humidified 5% CO_2 atmosphere. Incorporated tritiated thymidine was counted with a liquid scintillation counter (TopCount NXT; PerkinElmer Life Sciences, Boston, Mass). The stimulation index was calculated as milk protein–specific tritiated thymidine uptake (cpm)/vehicle-induced tritiated thymidine uptake (cpm).

Culture supernatants were harvested at day 6, and the cytokine production profiles were investigated by using Luminex multiplex cytokine analysis kits (Millipore) and ELISA (R&D Systems).

The lymphoproliferation assays and cytokine production assays were performed in duplicates and triplicates, respectively.

There was a significant positive correlation between the IL-2 concentration in the PBMC culture supernatant and lymphoproliferation (stimulation index) after stimulation with κ-casein ($r = 0.269$, $P = .025$; see Fig E2). Similar tendencies were also found when PBMCs were stimulated with other milk protein preparations (data not shown).

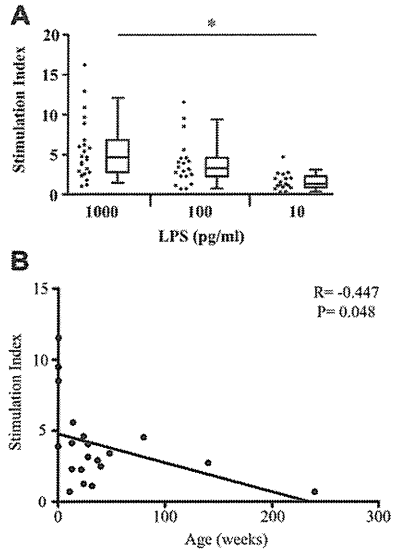

FIG E1. A, LPS at as little as 10 pg/mL can induce lymphoproliferation. PBMCs from young children (n = 60, 0-60 months of age) were stimulated with various concentrations of LPS (Sigma) for 5 days. Lymphoproliferation was measured by using tritiated thymidine uptake. The stimulation index was calculated as milk protein–specific tritiated thymidine uptake (cpm)/vehicle-induced tritiated thymidine uptake (cpm). $*P < .05$. **B,** LPS-induced lymphoproliferation was inversely associated with age. PBMCs from young children (n = 21, 0-240 weeks of age) were stimulated with 100 pg/mL LPS (Sigma) for 5 days. Lymphoproliferation was measured by using tritiated thymidine uptake. The stimulation index was calculated as milk protein–specific tritiated thymidine uptake (cpm)/vehicle-induced tritiated thymidine uptake (cpm).